Assessing the Impacts of Land Use and Land Cover-Based Drought Adaptation Measures with an Eco-Hydrological Model

Sven F. Grantz[1], Paul D. Wagner[1], Jens Kiesel[1,2], Nicola Fohrer[1]

[1] Department of Hydrology and Water Resources Management, Institute for Natural Resource Conservation, Kiel University, Kiel, Germany
[2] Stone Environmental, 535 Stone Cutters Way, Montpelier, VT 05602, USA

Correspondence to: sgrantz@hydrology.uni-kiel.de

Abstract. Europe has warmed by about 1.5 °C above pre-industrial levels and endured record-breaking droughts from 2018–2020, underscoring the need for adaptation to water scarcity. This study examines the potential of targeted land use and land cover (LULC) changes to modify water fluxes and soil moisture storage for greater hydrologic drought resilience. Evaluated measures comprise replacing grain corn with sorghum on agricultural fields, converting coniferous forests (spruce, pine) to broadleaved stands (beech, oak), and mitigating imperviousness in built-up areas.

The study area, the 1,983 km² Upper Lippe catchment in Germany, and the exceptionally dry period of 2011–2020, are suitable conditions to address the research question for a temperate region. The assessment was conducted with the eco-hydrological model SWAT+ and novel approaches were implemented to accurately parameterize agricultural land use and management, dominant tree species, and the realistic impervious fraction of built-up areas within the model using publicly available existing data products and studies. After applying a calibration strategy that specifically targeted low-flow periods, the model performs well in the study period combining a good representation of low-flow periods with a standardized Root Mean Square Error for flows exceeding a 70 % probability threshold of 0.14 and while also maintaining robust overall streamflow dynamics with a modified Kling-Gupta Efficiency (KGE') of 0.90 at the catchment outlet. The parameterization and calibration approaches can serve as references for model setups addressing similar ecoregions and research questions.

In the adapted agricultural areas, the evapotranspiration coefficient decreased by -11.7 percentage points (pp, area weighted median of the annual average) with reductions concentrated in the vegetation period leading to increases in soil moisture content. In response, the drainage flow coefficient increased by +3.3 pp with increases concentrated in the winter months and the groundwater recharge coefficient increased by +4.8 pp with a relatively uniform distribution throughout the year. The evapotranspiration coefficient from the adapted forested areas was reduced by -15.9 pp (from 67.5 %) with reductions occurring outside of the summer months. Here, increased soil moisture content increases the lateral flow coefficient by +9.0 pp and the groundwater recharge coefficient by 3.8 pp. Surface runoff increases only slightly, with enhanced surface runoff primarily occurring in mountainous areas where broadleaf trees provide less rainfall interception during winter dormancy. In the adapted built-up areas, reductions in impervious surfaces led to an increased groundwater recharge coefficient (+ 0.4 pp) and a decreased surface runoff coefficient (-3.6 pp), while the evapotranspiration coefficient increased (+2 pp), particularly in summer. Plant-available moisture in the topsoil increased in the adapted agricultural and forested areas across all modeled adaptation measures, reducing magnitude and duration of water stressed periods. These results

demonstrate that LULC adaptations can shift landscape water balance by reducing evapotranspiration and

40 increasing infiltration, thereby strengthening drought resilience and offering co-benefits such as urban cooling. Such insights can guide policy and land management toward scalable, land use-based solutions for extreme weather resilience under a warming global climate.

1 Introduction

Increased atmospheric temperature alters the hydrologic and energy cycles of the earth (Srivastav et al., 2021) and

45 influences the frequency, duration, intensity and spatial extent of extreme weather events such as heavy rainfall and prolonged periods of drought on the global scale. Europe is the fastest warming continent (European Environment Agency, 2024) and the frequency, intensity and duration of heatwaves have increased with the observed climate change in the past (Lorenz et al., 2019). Between 2006 and 2015, temperatures in Europe were already about 1.5 °C higher compared to the pre-industrial level (European Environment Agency, 2017) and the

50 continent has experienced extreme drought conditions from 2018 to 2020 which occurred with unprecedented intensity (Boergens et al., 2020; Hari et al., 2020; Rakovec et al., 2022) providing further evidence that droughts are exacerbated by climate change (Hari et al., 2020; Samaniego et al., 2018; Field et al., 2012). The variability in rainfall as well as the frequency and magnitude of droughts are predicted to increase further depending on the extent of global warming and its regional effects (Field et al., 2012; Samaniego et al., 2018; Hari et al., 2020;

55 Grillakis, 2019) which poses major challenges to water management, agricultural productivity and ecologic communities. Land use change has noticeable effects on water balance components such as runoff and water retention in storages such as soils and aquifers (Herrmann and Wendland, 2021; Wagner et al., 2023). As a result, they also affect droughts and floods and are therefore part of the problem of hydrologic extremes as well as part of the solution to their mitigation (Auerswald et al., 2024). Consistent with these findings, the first German

60 National Water Strategy from 2023 defines both a natural water balance and a climate adapted and water-efficient land use in agricultural, forested and built-up areas as key strategic goals (Bundesministerium für Umwelt und Naturschutz, nukleare Sicherheit und Verbraucherschutz, 2023). This study contributes to the knowledge base for land management and policy by investigating the hydrologic impacts of scalable, land use–based solutions aimed at enhancing drought resilience by increasing water retention in the landscape.

65 Droughts refer to periods of time with reduced water availability (Mishra and Singh, 2010) originating from substantially below-average climatic water balances driven by low precipitation and high temperatures resulting in negative impacts for various components of natural systems and socio-economic sectors (Ault, 2020; Wilhite et al., 2017). Depending on their duration, droughts propagate from meteorological phenomena to soil moisture droughts, during which plants experience water stress – also termed agricultural droughts when crop production is

70 affected – and hydrologic droughts, marked by relatively low surface and groundwater levels as well as reduced streamflow (van Loon, 2015; Menzel, 2016) as drainage from storages in the affected catchments is not sufficiently replenished.

A fundamental aspect of a system's resilience is its capacity to absorb disturbances while maintaining essential structure and function (Holling, 1973; Walker et al., 2004). In this study, droughts constitute disturbances and the

75 central function of a hydrologic system that needs to persist is its provisioning of water to connected systems. In particular, consistent streamflow and water levels as well as groundwater recharge affect socio-economic water supply (Marx et al., 2018; van Vliet et al., 2016) and aquatic habitats (Riedel et al., 2021; Kakouei et al., 2018).

Sufficient soil water content on the other hand has impacts on agricultural and forestry productivity (Jarrett et al., 2023) and terrestrial ecosystems (Salomón et al., 2022). Drought resilience of a hydrologic system is therefore the degree to which it provides sufficient water to meet the requirements of the socio-economic and ecological systems to which it is connected during periods of relative water scarcity and thus avoiding a propagation of the drought. The stabilization of water availability under drought conditions can be promoted by slowing down runoff processes, increasing the natural or artificial storage volume in the catchment and improving water efficiency of the dependent systems. In this study, we assessed the potential of land use and land cover (LULC, in this publication universally referred to as "land use") to increasing water retention in the landscape by reducing evapotranspiration and strengthening water fluxes through storages with long or medium residence times. Specifically, we investigated which hydrologic alterations are caused by adaptations in agricultural, forested, and built-up areas in a study period dominated by dry and extremely dry meteorological conditions as identified with the Standardized Precipitation and Evaporation Index (SPEI).

To assess the hydrologic impacts and the effectiveness of climate adaptation measures, field experiments as well as modeling studies can be used (Meyer et al., 2019). Hydrological models allow to understand the interactions of climate, topography, soil and land cover and their impacts on the water balance on the catchment scale, as well as to assess possible outcomes of land management strategies under different climatic conditions (Čerkasova et al., 2023; Parajuli et al., 2016; Kiniry et al., 2008). Therefore, modeling approaches are frequently used as an alternative or in addition to empirical studies (Liang et al., 2023). With their ability to model scenarios for large areas, modeling can assist policy design and administration (Čerkasova et al., 2023). Comprehensive eco-hydrological models like the Soil and Water Assessment Tool (SWAT) are particularly suited to assess the effects of land use-based climate adaptation measures on the landscape water balance, as they are capable of accurately representing different plants within the same land use class and evaluating how management and conservation practices affect water resources on the landscape scale (Čerkasova et al., 2023). In this study, SWAT+ (Arnold et al., 1998; Bieger et al., 2017) the latest, extensively restructured version of the model SWAT (Arnold et al., 1998) was used to assess changes in the water balance of the adapted areas in the upper Lippe catchment in Germany.

SWAT has already been successfully used to model the effects of various land use and management practices under different climate change scenarios (Parajuli et al., 2016; Bernini et al., 2023; Berihun et al., 2023; Hoque et al., 2014). A small number of studies investigate the effects of changes in isolated land use or land management categories (e.g. Yang et al., 2024; Eini et al., 2023; Gautam and Corzo, 2023; Kassaye et al., 2024; Nauta et al., 2024; Paez-Trujillo et al., 2023; Naik and Abiodun, 2024) on the water retention capacity for drought management with SWAT+. In this study, we follow a comprehensive approach by assessing adaptations in the three main land use categories agriculture (corn to sorghum), forested (coniferous to broad-leafed trees) and built-up areas (reduction of imperviousness). With detailed spatial discretization and model parameterization, a realistic representation of the current state of these areas was established and changes are analyzed separately for the distinct land uses across the different site conditions to investigate their respective potential as measures for increasing drought resilience.

2 Materials and Methods

2.1 Catchment description

115   The study area is the upper Lippe catchment limited by the gauging station Kesseler 3 which is situated 152.9 km upstream from the Lippe's confluence with the Rhine River. It comprises an area of 1,983.6 km^2 and accounts for 41 % of the entire Lippe catchment which is located in the state of North Rhine Westphalia in the West of Germany. The mean discharge of the river at the outlet of the study catchment at 63,6 m.a.s.l is 22,2 m^3/s (1991-2020) with

120   a coefficient of variability of 79 % (Ministerium für Umwelt, Naturschutz und Verkehr NRW, 2024). The mean elevation of the upper Lippe catchment is 213.6 m.a.s.l with a minimum elevation of 35.7 m.a.s.l and a maximum elevation of 614.4 m.a.s.l comprising both mid-range mountain and lowland areas as shown in Fig. 1a. The study area has a population size of 451,387 according to the census 2022 (Statistisches Bundesamt - Destatis, 2023) resulting in a population density of 227 inhabitants per km^2.

125   Land use of the study area shown in Fig. 1b is dominated by agriculture with 51 % of the catchment being used as rainfed agricultural land and 13 % as grassland (European Environment Agency, 2020a). The most frequently cultivated crops are corn, winter grains (barley and wheat), and rapeseed, which are mainly grown in rotation, with some corn monocultures still prevalent (Landwirtschaftskammer Nordrhein-Westfalen, 2023). Forests in the upper Lippe catchment cover 24 % of the area and spruce and beech dominate in the mid-range mountains where the

130   eastern and south-eastern headwaters of the Lippe are situated (Blickensdörfer et al., 2024). In the lowlands, oak is dominant throughout the catchment while the region in the north-east of the catchment contains a distinct pine agglomeration (Blickensdörfer et al., 2024). Built up-areas account for 9 % of the study area and are used for settlements (7 %) as well as industrial and commercial purposes including transportation (2 %). There are 25 reservoirs located in the upper Lippe catchment with a total retention volume of approximately 2,500 million m^3

135   which are mainly operated for flood control and some water supply purposes (Wasserverband Obere Lippe, 2024). The soils of the upper Lippe catchment (Geologischer Dienst NRW, 2023) are dominated by loamy and textures south of the Lippe River and in the eastern mid-range mountains (Fig. 1c) with higher runoff and lower infiltration potential. The lowlands of the Westphalian Basin north of the Lippe River are in contrast dominated by sandy loam and loamy sand soils with medium infiltration potential while the sandy soils of the region in the north-east

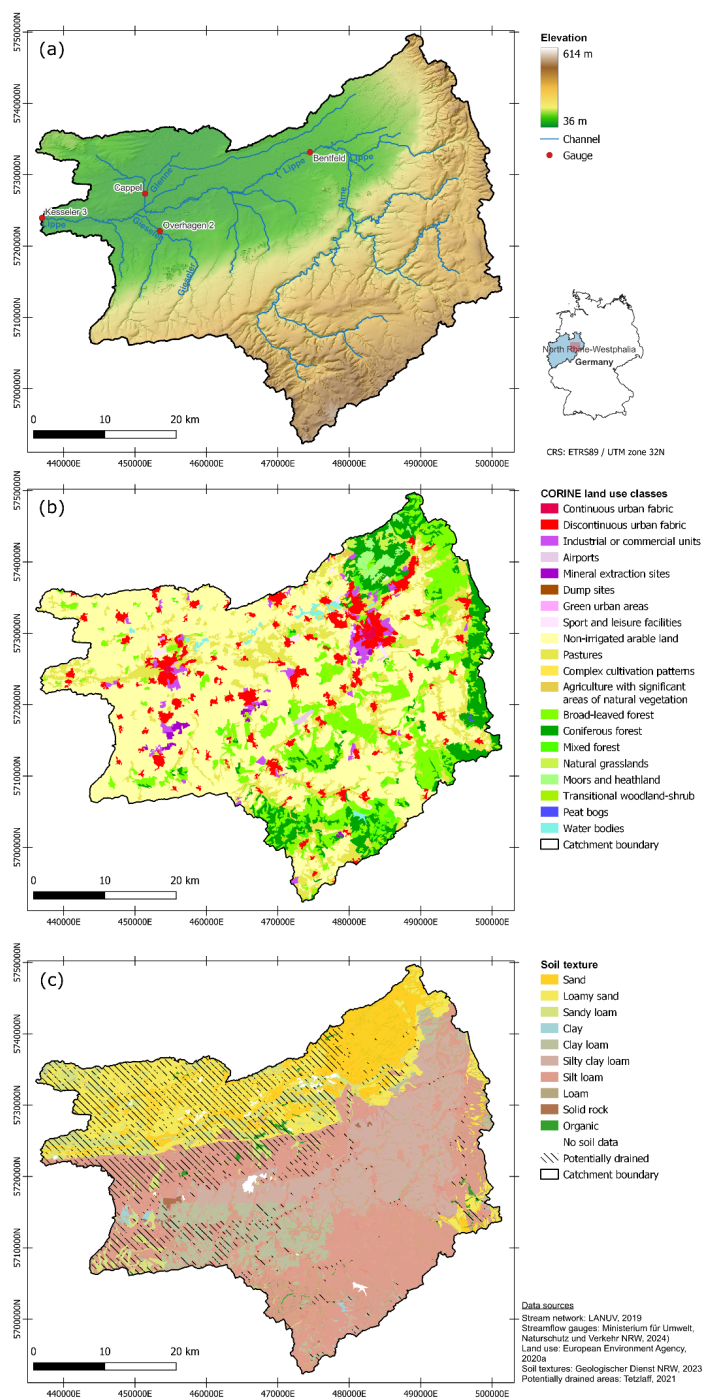140   have the highest infiltration potential.

Figure 1: (a) Topography with stream network (LANUV, 2019) and streamflow gauges (Ministerium für Umwelt, Naturschutz und Verkehr NRW, 2024), (b) spatial distribution of CORINE 2018 land use classes (European Environment Agency, 2020a), (c) soil textures (Geologischer Dienst NRW, 2023) and potentially drained areas (Tetzlaff, 2021) of the upper Lippe catchment

145

5

2.2 Meteorological input data and climatic trend analysis

We used daily precipitation and temperature data from the HYRAS data set – a high-resolution gridded observational weather dataset for Central Europe (Razafimaharo et al., 2020; Rauthe et al., 2013) provided by the German Weather Service (Deutscher Wetterdienst, 2022). We conducted statistical tests on the annually

150   aggregated weather data to identify potential climate trends in the period from 1991 to 2020 (Fig. 2). The Mann-Kendall trend tests (Mann, 1945; Kendall, 1955), conducted with the R-package "trend" (Pohlert, 2023) showed that the null hypotheses for no trends in precipitation (p-value = 0.008) and average temperatures (p-value = 0.010) can be rejected with statistical significance. Annual precipitation sums exhibit a negative trend with a Sen's slope (Sen, 1968) of -8.48 mm / year while annual average temperatures are rising with a Sen's slope of 0.034 °C / year.
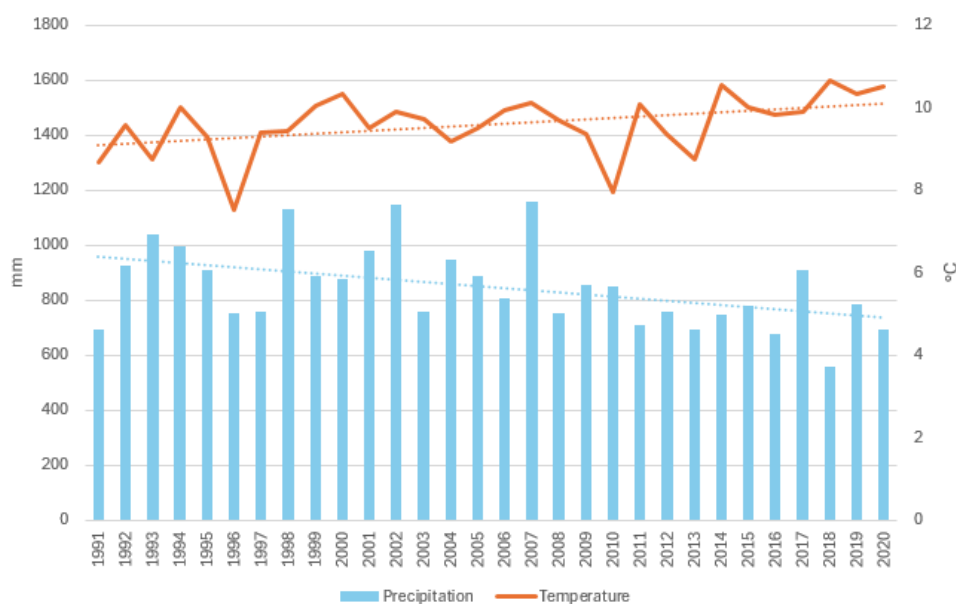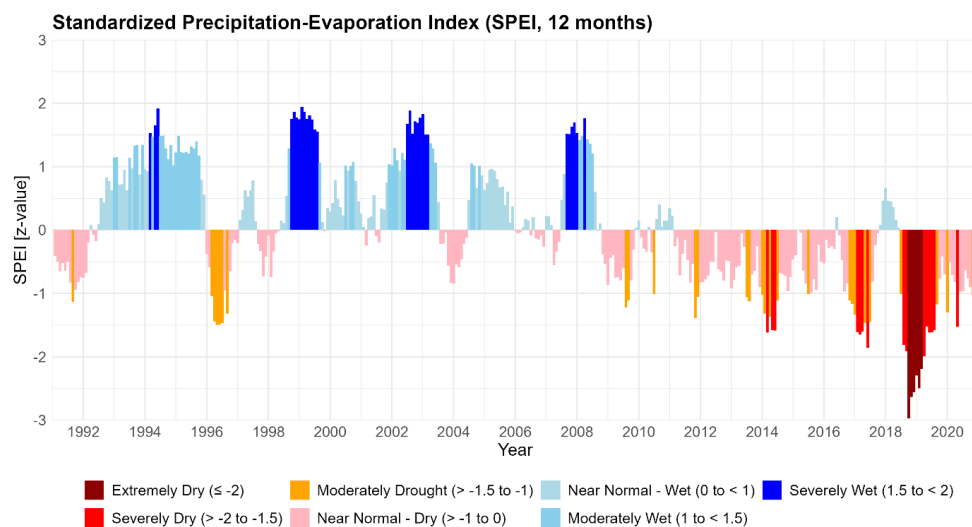

155

Figure 2: Climate trends in the upper Lippe Catchment (1991 – 2020) with linear trendlines and Sen's slopes

The Standardized Precipitation-Evaporation Index (SPEI) is a statistical indicator that identifies dry and wet periods based on the climatic water balance as the difference between total precipitation and the sum of potential evaporation aggregated on different time scales (Vicente-Serrano et al., 2010). It builds on the concept of the

160   Standardized Precipitation Index (SPI) developed by McKee et al. (1993) but captures water deficits or water surpluses of the land surface better by considering the impact of temperature variability on evaporative water demand while preserving the robust statistical features of the SPI. Like the SPI, the SPEI can be calculated on a range of timescales from 1-48 months. We analyzed the SPEI for the upper Lippe Catchment with the R package "SPEI" (Beguería and Vicente-Serrano, 2023) with an aggregation period of 12 months and potential evaporation

165   calculated with the Hargreaves method (Fig. 3). This analysis shows that the period following 2009 was almost exclusively characterized by relative dryness.

Standardized Precipitation-Evaporation Index (SPEI, 12 months)

Legend:
- Extremely Dry (≤ -2)
- Severely Dry (> -2 to -1.5)
- Moderately Drought (> -1.5 to -1)
- Near Normal - Dry (> -1 to 0)
- Near Normal - Wet (0 to < 1)
- Moderately Wet (1 to < 1.5)
- Severely Wet (1.5 to < 2)

Figure 3: Standardized Precipitation-Evaporation Index (12 months) – upper Lippe Catchment, 1991 – 2020 with SPEI thresholds from Deutscher Wetterdienst (n.d.)

2.2 Eco-hydrological Model

The eco-hydrological model SWAT+ (Arnold et al., 1998; Bieger and Arnold, 2017), of which we used version 60.5.4, is a completely revised version of the SWAT model (Arnold et al., 1998; Arnold and Fohrer, 2005). It divides the catchment into subcatchments which contain a channel and are further divided into Hydrologic Response Units (HRUs) – spatial entities with unique soil, land use and slope combinations. For each HRU, changes in soil water storage along with the processes of evaporation, surface runoff, lateral and drainage flow as well as percolation are calculated on a daily time step. Water leaving the HRUs via surface runoff, lateral and drainage flow is directly received by the modeled channel where the water is routed to the subcatchment outlet. Water percolating from HRUs enters shallow aquifers and – after optional subtraction of losses to a deep aquifer or due to capillary rise and plant uptake – discharged as groundwater flow to the respective channel.

For the delineation of the catchment and the derivation of slope classes, a digital elevation model (DEM) with a 10 m resolution (Fig. 1a) resampled with bilinear interpolation from a 1 m raster dataset (Landesvermessung NRW, 2023) was used. Four slope classes were defined with class borders based on the USDA Soil Survey Manual (United States Department of Agriculture, 2017) at 3 %, 8 % and 16 %. A river network map based on the official water bodies map of North Rhine-Westphalia (LANUV, 2019) was used and the threshold for stream and channel definition was set to 25 km^2 resulting in the modeled river network shown Fig. 1a. A soil map with a resolution of 1:50,000 and soil parameters produced in accordance with the German soil mapping guidelines of the Bundesanstalt für Geowissenschaften und Rohstoffe (2005) by the State Geological Service of North Rhine-Westphalia (2023) were used as model inputs (Fig. 1c). The soil hydrologic groups additionally required by the SWAT+ model were estimated with pedotransfer functions in accordance with United States Department of Agriculture (2009) specifications. The HRU generation considered land uses accounting for more than 2 %, soils for more than 11 % and slope classes for more than 10 % of each subcatchment to filter out very small unique combinations. The areas of the filtered HRUs were redistributed proportionately to the generated HRUs within each subcatchment.

195   The weather data used as input to the model were daily minimum and maximum temperature (Razafimaharo et al., 2020) and daily precipitation (Rauthe et al., 2013) from the above described HYRAS dataset. Potential evapotranspiration was calculated with the method of Hargreaves and Samani (1985).

2.2.1 Land use classification and parameterization

The models' land use data comprises combined information from several datasets. The CORINE Land Cover 2018
200   product with a minimum threshold of 25 ha for areas to be categorized as singular land use units (European Environment Agency, 2020a) serves as a base layer (Fig. 1b). A more detailed spatial representation and parametrization of agricultural land use and the identification of common crop rotations were derived from data of the Integrated Administration and Control System (IACS) for the implementation of the European Union's Common Agricultural Policy (CAP). This database is used as a basis for EU grant processing and contains annual
205   data on crops on the field scale. For the Lippe catchment this high-resolution dataset was provided for the years 2016 to 2022 by the Chamber of Agriculture of North Rhine-Westphalia (Landwirtschaftskammer Nordrhein-Westfalen, 2023). This complex approach allowed for accurate spatial representation of the current agricultural land use on the field scale combined with generalized crop rotation schedules that are conducive to exploring land use scenarios.

210   The modeled crop rotations with sowing and harvesting as well as tillage operations were added as management schedules. Management operations for grain sorghum are based on the information of field trials in Germany (Bayerische Landesanstalt für Landwirtschaft, 2024). Harvesting and tillage parameters (Appendix 1, Tables A1 and A2) were adjusted according to standard German agricultural practices (Kuratorium für Technik und Bauwesen in der Landwirtschaft, 2009). The planting and sowing dates were adjusted based on phenology data
215   from the German Weather Service (Deutscher Wetterdienst, 2023). Management operation dates and parameters were subsequently verified and adjusted based on the regional conditions and common practices derived from an expert interview with the Chamber of Agriculture of North Rhine-Westphalia (2024). In the model, cover crops are uniformly represented by red clover. According to regional practices, cover crops are planted before corn in all crop rotations while no cover crops are planted with corn monocultures. The final management schedule of the
220   model contains the operations shown in Table A3 of Annex 1.

Drainages are represented in the model based on the spatial distribution of potentially drained areas in North Rhine-Westphalia estimated by Tetzlaff (2021) and shown in Fig. 1c. Agricultural fields that were at least 30 % potentially drained were classified as tile drained. To calculate drainage flow, the original tile drainage equation of SWAT is used (Neitsch et al., 2011). This method considers the perched water table and simulates the tile flow
225   on days when the height of the perched water table layer is greater than the height of the tile (Du et al., 2005). It considers the following three user defined parameters in SWAT+ (v. 60.5.4). The depth of the tile drainages was set to 800 mm in accordance with the assumptions of a water balance model for North Rhine-Westphalia (Herrmann and Wendland, 2021) which were confirmed as generally plausible by the Chamber of Agriculture of North Rhine-Westphalia (2024). The time to drain the soil to field capacity in hours and the maximum daily
230   drainage capacity in millimeters are used as calibration parameters.

As a basis for the modeling adaptation in forested areas we further refined the spatial representation and parameterization of forests in the model. For areas classified as forested in the CORINE 2018 land cover map (European Environment Agency, 2020a) the most prevalent tree species groups were identified based on a map product from the Thünen-Institut (Blickensdörfer et al., 2022). This novel dataset combines remote sensing time

series (Sentinel-1 and -2) with sample-based data from the German National Forest Inventory and environmental data to generate a map of dominant tree species covering the whole German territory with a spatial resolution of 10 m (Blickensdörfer et al., 2024). Several studies have shown that the default SWAT plant database is insufficient to correctly model the water balance of forested areas (Haas et al., 2022; Karki et al., 2023; Yang and Zhang, 2016). Therefore, SWAT+ tree parameters for oak *(Quercus spp.)*, beech *(Fagus sylvatica)*, birch *(Betula spp.)*, pine *(Pinus spp.)*, spruce *(Picea spp.)* and douglas fir *(Pseudotsuga menziesii)* identified for Germany and published by Müller (2022) were used in this study.

The model setup for this study distinguishes the two land use classes of partially impervious built-up areas which were delineated based on the CORINE 2018 land cover map. The model's "settlements" class comprises the CORINE land cover classes Continuous Urban Fabric, Discontinuous Urban Fabric, Green Urban Areas, Sport and Leisure Facilities. Areas in the CORINE classes Industrial or Commercial Units as well as transport classes are lumped in the model's "industry and commerce" class. The model calculates runoff based on the SCS Curve Number Method (USDA Soil Conservation Service, 1972) and assigns an SCS curve number of 98 to the fraction of impervious surfaces while the hydrologic properties of the unsealed fraction is calculated based on its land use and soil type (Neitsch et al., 2011). To achieve a realistic representation of the built-up areas in the model, the fraction of impervious surfaces has been identified using a map product containing information on imperviousness density (European Environment Agency, 2020b). This raster dataset contains estimates of impermeable cover of soil for Europe at a resolution of 10 m derived from analysis of Sentinel-2 satellite imagery. The identified mean impervious fractions in the study catchment are 0.46 for settlements and 0.58 for industrial and commercial areas, respectively.

2.2.2 Model calibration and validation

The aim of the calibration strategy was to optimize the water balance and discharge dynamics of the entire upper Lippe catchment with a particular focus on low-flow periods. Thus, the observed daily average discharge at the catchment outlet at gauge Kesseler 3 (Fig. 1a) from 2001 to 2020 (Ministerium für Umwelt, Naturschutz und Verkehr NRW, 2024) was used for the calibration of the SWAT+ model of the upper Lippe catchment. Further discharge measurements at the station Bentfeld as well as the subcatchments of the Gieseler with gauge Overhagen 2 and of the Glenne gauged at Cappel (Fig. 1a) are used for additional spatially distributed model validation. Due to the above identified decreasing trend in precipitation, the calibration and validation periods were defined to equally include wet and dry years (Table 1).

Table 1: Separation of the calibration and validation periods

	Calibration Period	Validation Period
Years (sorted by precipitation, high to low)	2007, 2018, 2004, 2013, 2005, 2014, 2010, 2003, 2019, 2015	2002, 2016, 2001, 2020, 2017, 2011, 2009, 2008, 2006, 2012
Average annual precipitation	814 mm	827 mm
Standard deviation of precipitation	153 mm	141 mm

In an initial step, the model's bias between observed and simulated discharge was assessed to evaluate the plausibility of the water balance. The applied performance metric was Percent Bias (PBIAS), which quantifies the deviation between observed and simulated datasets as a percentage where positive PBIAS values indicate model

270 overestimation and negative values signify underestimation (Yapo et al., 1996; Sorooshian et al., 1993). Initially, the SWAT+ model of the upper Lippe catchment exhibited an underestimation of the modeled streamflow with a PBIAS of -33.8 in the calibration period at the catchment outlet (gauge Kesseler 3). The recharge coefficient to the deep aquifer which represents losses from the system (Neitsch et al., 2011) and was set to 0 (SWAT+ default value = 0.05) assuming that no water is lost from the catchment resulting in a PBIAS of -29.3. To adjust the

275 evapotranspiration with the aim to achieve plausible runoff quantities, here defined as -10 ≤ PBIAS ≤ 10, before automatic calibration, the calibration coefficient of the Hargreaves potential evaporation equation (Hargreaves and Samani, 1985) was adjusted to 0.0018 resulting in a PBIAS of -9.9.

Following these preliminary manual parameter adjustments 19,200 parameter sets were generated by Latin Hypercube Sampling (Soetaert and Petzoldt, 2010; McKay, 1988; McKay et al., 2000) using the parameter ranges

280 shown in Table 2 for automatic calibration. The selected calibration parameters cover the models' relevant conceptualized components of the hydrologic cycle including evaporationtranspiration (*esco, epco*) surface runoff (*surlag, cn2, cn3_swf*), lateral flow (*latq_co*), tile flow (*tile_dtime, tile_drain)* as well as groundwater recharge (*perco*) and retention (*alpha*). The parameter set furthermore comprises the physical properties of the soil (*bd, awc, k*) as well as of the aquifer's specific yield (*sp_yld*). The parameter ranges for the conceptual parameters *esco,*

285 *epco, latq_co* and *perco* extent to the maximum possible ranges of the SWAT+ model while the minima and maxima of the remaining parameters were limited based on prior sensitivity tests. For each parameter set a model run was performed.

The modified Kling-Gupta Efficiency (KGE') was applied as the first objective function for attaining a good model representation of overall streamflow dynamics as it optimizes the Euclidian distance in a three-dimensional

290 parameter space between the correlation coefficient, the bias ratio and the variability ratio (Kling et al., 2012). It has been found by Kling et al. (2012) to be superior to the widely used Nash-Sutcliffe Efficiency (NSE, Nash and Sutcliffe, 1970) which will only be considered here as additional information on model performance. The second objective function was the low-flow performance of the model measured by the Root Mean Square Error standardized using the standard deviation of the overserved discharge (Moriasi et al., 2007) applied to the low-

295 flow segment of the flow duration curve (Pfannerstill et al., 2014; Haas et al., 2016). In contrast to Haas et al. (2016) the low-flow segment in this calibration comprises flows with an exceedance probability of 70 % as categorized by Yilmaz et al. (2008) to lump both low- and very low-flows in one performance metric (RSR_Q70). Firstly, the 99th percentile of the model runs, sorted by KGE', were selected. Secondly, the selected runs were then ranked by RSR_Q70 to determine the optimal parameter set in accordance with the calibration strategy.

300 Calibration and validation were carried out in R using the packages FME (Soetaert and Petzoldt, 2010) and SWATrunR (Schuerz, 2024) for Latin Hypercube Sampling and hydroGOF (Zambrano-Bigiarini, 2024) for model evaluation and the packages zoo (Zeileis and Grothendieck, 2005) and xts (Ryan et al., 2024) for data processing.

Table 2: Calibration parameters, upper and lower boundaries and final values/adjustments

Parameter	Description	Change	Min	Max	Final change value
surlag	Surface runoff lag coefficient	absval[1]	0.05	1	0.051
cn2	Condition II curve number	abschg[2]	-30	2	-4.678
cn3_swf	Soil water factor for curve number condition III	absval[1]	0	1	0.468
esco	Soil evaporation compensation coefficient	absval[1]	0	1	0.341
epco	Plant water uptake compensation coefficient	absval[1]	0	1	0.945
awc	Available water capacity of the soil layer (mm H_2O/mm soil)	pctchg[3]	-20	20	-13.647
k	Saturated hydraulic conductivity of soil layer (mm H_2O/hr)	pctchg[3]	-50	50	38.602
bd	Bulk density of soil layer (Mg/m^3 or g/cm^3)	pctchg[3]	-30	20	-10.615
latq_co	Lateral flow coefficient	absval[1]	0	1	0.461
tile_dtime	Time to drain soil to field capacity (hrs)	absval[1]	48	72	50.200
tile_drain	Maximum drainage capacity per day (mm)	absval[1]	10	51	32.951
perco	Percolation coefficient	absval[1]	0	1	0.610
alpha	Baseflow recession constant	absval[1]	0.001	0.2	0.007
sp_yld	Aquifer specific yield (m^3 H_2O/m^3)	absval[1]	0.05	0.2	0.081

305 [1] *absval* replaces the initial parameter value with an absolute value.

[2] *abschg* adds an absolute value to the initial parameter value.

[3] *pctchg* changes the initial parameter value by a percentage.

2.3 Land use scenarios

310 To assess the hydrologic effects of climate adaptation measures, an alternative land use scenario was created which comprises three different adaptation categories affecting five land use classes:

1. Crop adaptation: To model the effects of this adaptation in the study catchment, agricultural areas where grain corn [*Zea mays* L.] is cultivated – either as monoculture or as part of crop rotations – it is replaced by grain sorghum [*Sorghum bicolor* (L.) Moench]. To increase the number of evaluated years to the full

315 investigation period, crop rotations were modeled as corn monocultures in the base scenario and grain sorghum monocultures in the adaptation scenario. This conversion affects 120.8 km², accounting for 6.2 % of the modeled watershed. The rationale for this adaptation is the higher water efficiency and water

11

stress resilience of sorghum compared to corn found in field experiments (Bhattarai et al., 2020; Jahansouz et al., 2014). In Germany, sorghum was grown on a total area of 11,000 ha in 2020, primarily in drought affected areas and as an energy crop (Bockholt, 2020). Field trials in Northern Bavaria confirmed that yields of sorghum are below to those of corn when sufficient water is available but become comparable under water limited conditions (Bayerische Landesanstalt für Landwirtschaft, 2024).

2. Forest composition adaptation: This adaptation category is based on findings from field experiments with large lysimeters in Germany that show that evapotranspiration from broad leafed trees is notably lower than from coniferous trees (Müller, 2005; Landesamt für Natur, Umwelt und Verbraucherschutz, 2018; Harsch et al., 2009; Müller, 2011). In forested areas which account for 8.8 % of the modeled watershed, the replacement of coniferous by broad-leaved tree species was modeled. Areas currently dominated by spruce were converted to beech-dominated areas and pine-dominated areas are converted to oak-dominated areas.

3. Imperviousness adaptation: The climate adaptation scenario contains a reduction of imperviousness in built-up areas which account for 9.1 % of the modeled catchment area. For urban areas, the impervious fraction was reduced by 13 percentage points to 33 % and for industrial and commercial areas (including large transport infrastructure) the impervious fraction was reduced by 15 percentage points to 43 %. This adaptation was based on findings of previous studies that reductions of sealed surfaces can improve infiltration and that green infrastructure, such as permeable surfaces or vegetated buffers, can mitigate runoff and promote groundwater recharge (Zölch et al., 2017; Sohn et al., 2020).

The detailed changes from the status quo, the "baseline scenario", to the "adaptation scenario" are shown in .

Table 3 which also defines the short names for the measures based on the initial land use in the baseline scenario and used for further reference and spatially depicted in Fig. 4.

Table 3: Overview of modeled land use adaptation measures

Category	Land use "Baseline scenario"	Land use "Adaptation scenario"	Short name	Area [km²]	Share of catchment area [%]	HRUs [quantity]
Agriculture	Grain corn	Grain Sorghum	CORN_SORGHUM	94.6	6.2	158
Forest	Spruce	Beech	SPRUCE_BEECH	125.6	6.3	116
	Pine	Oak	PINE_OAK	48.9	2.5	30
Built-up areas	Settlements (46 % imperviousness)	Settlements (33 % imperviousness)	URBAN_IMP	143.5	7.2	337
	Industry and Commerce (58 % imperviousness)	Industry and Commerce (43 % imperviousness)	INDUSTRY_IMP	38.3	1.9	72

12
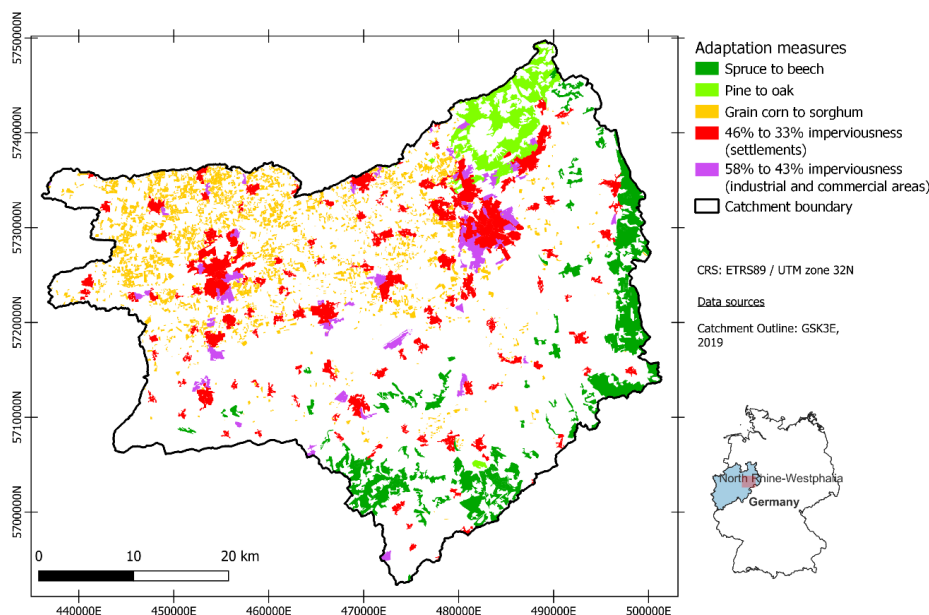
345   **Figure 4: Spatial distribution of modeled adaptation measures**

2.3 Assessment of hydrologic impacts

To assess the hydrologic impacts of the land use changes, we analyzed the differences in the water balance components of the adapted HRUs in the study period from 2011 to 2020. The evaluation was carried out at both annual and monthly scales. To account for the different areas of the HRUs, the evaluation metrics for the changed

350   land use classes or adaptation categories were spatially aggregated by calculating their respective area-weighted medians.

The examined hydrologic fluxes comprised actual evapotranspiration, surface runoff, tile drainage flow, lateral flow, soil water storage change and groundwater recharge. Reductions in evapotranspiration are considered beneficial to water retention in the landscape. Soil and groundwater storages have comparably longer residence

355   times than surface water bodies (Weiler and Miegel, 2016). Tile drainage flow primarily forms a fast flow component (Northcott et al., 2002). Accordingly, increases in lateral flow, soil water change and groundwater recharge are considered to increase water retention whereas increases in surface runoff and tile drainage flow are considered to decrease water retention.

We investigated the annual averages of the fluxes [mm] of the changed HRUs as well as the flux coefficients,

360   normalized by precipitation to aggregate across regions with different precipitation levels as shown in the following formula:

$$C_{F,i} = \left(\frac{\bar{\bar{F}}_i}{\bar{P}_i} \right) \times 100$$

where $C_{F,i}$ is the normalized flux coefficient [%] for HRU i, F_i is the annual hydrologic flux [mm] in HRU i averaged over the investigation period, P_i is the annual precipitation [mm] received by HRU i averaged over the

365   investigation period, and i denotes the index of the HRU within the investigated land use class.

13

The changes in flux coefficients were calculated at the HRU level using the following equation:

$$\Delta C_{F,i} = \left(\frac{\bar{F}_{i,adaptation} - \bar{F}_{i,baseline}}{\bar{P}_i} \right) * 100$$

where $\Delta C_{F,i}$ is the normalized change of the hydrologic flux coefficient for HRU i expressed in percentage points [pp], $F_{i,scenario}$ is the annual hydrologic flux [mm] in HRU i under the respective scenario averaged over the

370   investigation period, P_{HRUi} is annual precipitation [mm] received by HRU i averaged over the investigation period, and i denotes the index of the HRU within the investigated land use class.

For the analysis of the intra-annual progression of changes to the flux and state variables of the water balance, the changed land use classes were aggregated across the adaptation categories. To quantify the effects of the modeled land use changes on the hydrologic fluxes, differences in monthly values were calculated as follows:

375                            $$\Delta F_{i,m} = \bar{X}_{i,m,adaptation} - \bar{X}_{i,m,baseline}$$

where $\Delta F_{i,m}$ is the change of a hydrologic flux [mm] in HRU i in month m, $\bar{X}_{HRUi,m,scenario}$ is the monthly hydrologic flux [mm] in HRU i averaged over the investigation period under the adaptation and baseline scenarios, and i denotes the index of the HRU within the investigated adaptation category.

In addition to the water fluxes, the intra-annual progression of the hydrologic state variable soil water content was examined. To analyze the effects of the adaptation measures on soil moisture, the relative plant available water

380   content (RPWC) of the topsoil up to a depth of 300 mm was calculated for each month. The calculation of RPWC is based on the formula derived from UFZ Helmholtz Zentrum für Umweltforschung (2024) and adapted as follows:

$$RPWC_{i,m} = \left(\frac{\overline{SWC_{i,m}} - WP_i}{AWC_i} \right) * 10$$

385   where $RPWC_{i,m}$ is the plant available water [%] in HRU i during month m, $SWC_{i,m}$ is the soil water [mm] stored in HRU i during month m averaged over the investigation period, WP_i is the wilting point of the soil [mm] of HRU i and AWC_i is the plant available water capacity of the soil [mm] of HRU i, and i denotes the index of the HRU within the investigated adaptation category. For interpretation of this metric, common generalized thresholds are set at 50 % for mild water stress impairing plant development and 30 % for full-fledged water stress with

390   beginning wilting of plants (UFZ Helmholtz Zentrum für Umweltforschung, 2024).

3 Results

3.1 Model performance

The implementation of the calibration strategy led to the selection of the parameter set presented in Table 2 which achieved the optimal low-flow performance measured by RSR_Q70 (0.12) while ranking in the top 1 % (> 0.883)

395   for overall streamflow representation as measured by KGE' in the calibration period. A comparison of model performance metrics shown in Table 4 between the calibration and validation periods (Table 1) indicates that the calibrated model maintains a robust performance outside the calibration period for which the optimal parameter set was selected.

400 **Table 4: Model performance in the calibration, validation, and investigation period (2011 – 2020) at the catchment outlet Kesseler 3 and further gauges for spatial validation**

Period	Gauge	River	KGE'	PBIAS	NSE	RSR	RSR_Q70
Calibration	Kesseler 3	Lippe	0.89	-1.8	0.78	0.46	0.12
Validation	Kesseler 3	Lippe	0.90	2.9	0.80	0.45	0.26
Investigation	Kesseler 3	Lippe	0.90	-3.4	0.83	0.41	0.14
	Bentfeld	Lippe	0.74	23.5	0.75	0.50	0.43
	Cappel	Glenne	0.62	-0.9	0.70	0.55	0.51
	Overhagen 2	Gieseler	0.79	-10.3	0.76	0.48	0.36

In the investigation period from 2011 to 2020, the calibrated model exhibits a KGE of 0.90, PBIAS of -3.4 and an NSE of 0.83 at the main catchment outlet Kesseler 3 (Table 4). The flow duration curve (Fig. 6) shows a good
405 agreement of modeled and measured streamflow in all flow segments. The model performs best in the representation of the mid (20 % to 70 % exceedance probability) and very low flows (> 95 % exceedance probability) while the representation of very high flows (< 5 % exceedance probability) is comparatively weaker . Accordingly, the hydrograph (Fig. 5) shows a very good overall representation of discharge dynamics in the recession and low flow periods. The dynamics of extreme peak flows are represented correctly but their magnitude
410 is overestimated by the model. The performance metrics of the gauges of the subcatchment used for spatially distributed validation indicate an overall good representation of streamflow dynamics (Table 4). While being within an acceptable range, they also indicate an overestimation of the headwater's contribution (gauge Bentfeld) to the total discharge which is compensated by higher discharge quantities in the lower catchment when calibrating for the optimal performance for the whole catchment.
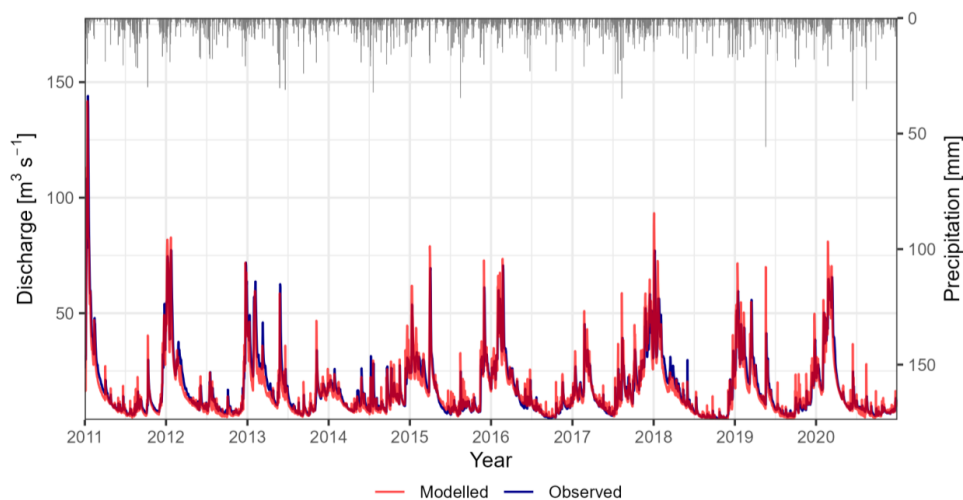
415

Figure 5: Comparison of the modeled and measured hydrographs at the catchment outlet (gauge Kesseler 3) in the investigation period 2011 – 2020 after model calibration
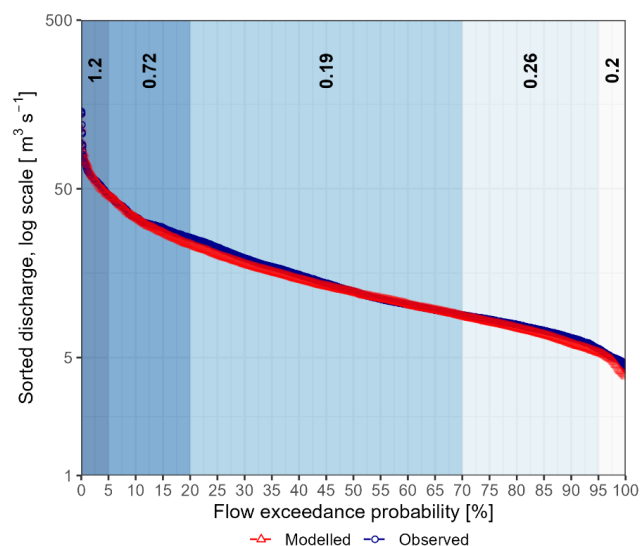
Figure 6: Comparison of the modeled and measured flow duration curves at the catchment outlet (gauge Kesseler 3) in the investigation period 2011 – 2020 after model calibration with RSR of the segments of the flow duration curve, segmentation in accordance with Pfannerstill et al. (2014).

3.2 Effects of land use adaptations on hydrologic fluxes and state variables

3.2.1 Changes to the annual water balance

We compared the modeled water balances from 2011 to 2020 of the areas which were changed between the baseline and the adaptation land use scenarios. The coefficients of evapotranspiration, direct runoff components and groundwater recharge relative to precipitation for each changed land use class which are used for the analysis and intercomparison of the effects of the land use changes are shown in Table 5 while Fig. 7 contains the underlying flux volumes.

Agricultural areas where corn is grown in the baseline scenario receive the least amount of precipitation per year (663 mm) compared to the investigated forested and urban areas and precipitation exhibits the least variance but evapotranspiration is much higher than in all other investigated land use classes. Most of the remaining water infiltrates the soil profile while surface runoff from these areas is minimal. Most of the infiltrated water percolates and recharges the groundwater storage whilst a lesser amount flows laterally through the soil profile or through drainages. The agricultural areas with corn cropping experienced the largest soil water storage losses throughout the investigation period compared to the other investigated land use classes. When the crop cultivated in these areas is replaced by sorghum (CORN_SORGHUM), the model results show a decrease in evapotranspiration by an area-weighted median of -11.7 pp which makes more water available for other fluxes. Here, the groundwater recharge experiences the greatest increase of +4.8 pp from crop adaptation while the lateral flow increases by +2.5 pp. Drainage becomes a notably more important flow path with an increase of +3.3 pp while surface runoff remains unchanged.

In the investigated forested areas, evapotranspiration is the dominant water flux but not as pronounced as in the investigated agricultural areas. Forest areas also receive the highest volumes of precipitation. Pine-dominated areas show a higher amount of evapotranspiration compared to spruce-dominated areas. In pine-dominated areas, groundwater recharge plays a higher role than lateral flow but the latter exhibits a higher spatial variability. No

16

surface runoff is generated from pine-dominated areas. Spruce-dominated forested areas in turn exhibit larger volumes of horizontal fluxes – through the soil profile as lateral flow as well as surface runoff – while still generating a fair amount of groundwater recharge. Both classes of forested areas show negative changes of soil water content during the investigated dry period but the losses are more pronounced in the pine dominated areas.

450 The replacement of coniferous with broad-leafed tree species causes evapotranspiration to strongly decrease in the changed areas. In areas where spruce trees are replaced by beech trees (SPRUCE_BEECH) evapotranspiration decreases by -15.7 pp while lateral flow increases most strongly (+9.9 pp) followed by groundwater recharge (+2.4 pp) and surface runoff (+1.6 pp). In areas where pine is replaced by oak (PINE_OAK) the reduction in evapotranspiration by -17.2 pp increases groundwater recharge most strongly (+10.7). Lateral flow increases by

455 +5.2 pp while surface runoff remains irrelevant in PINE_OAK areas. All investigated forested areas experience a reduction of average annual soil water depletion. Surface runoff, lateral flow and groundwater recharge show greater variance after adaptation.

The investigated built-up areas receive slightly more precipitation than the investigated agricultural areas but a lot less than the investigated forested areas. Evapotranspiration accounts for more than half of the received

460 precipitation. Most of the remaining water leaves the areas as surface runoff while a smaller fraction recharges the groundwater storage. Lateral flows are minimal. The built-up areas experience relatively small decreases in soil water storage. The reduction in imperviousness leads to reductions in surface runoff by -4.1 pp from the industrial and commercial areas (INDUSTRY_IMP) and -3.6 pp from the urban areas (URBAN_IMP). In turn, evapotranspiration increases by +2.6 pp from INDUSTRY_IMP areas and +1.9 pp from URBAN_IMP areas.

465 Groundwater recharge rises by +0.5 pp in INDUSTRY_IMP areas and +0.2 pp in URBAN_IMP areas. Soil water storage is slightly decreased +0.2 pp in INDUSTRY_IMP areas and +0.1 pp in URBAN_IMP areas. Lateral flows and the variance of the water fluxes are only minimally affected by the modeled reduction of imperviousness.

The maps shown in Fig. 8 depict the spatial distribution of the described changes with surface runoff, drainage flow and lateral flow summed to water yield. The maps highlight that changes do not only differ between the

470 adapted land use categories but also within the same category. These differences are related to spatial variance in meteorological variables, soil properties and slopes.
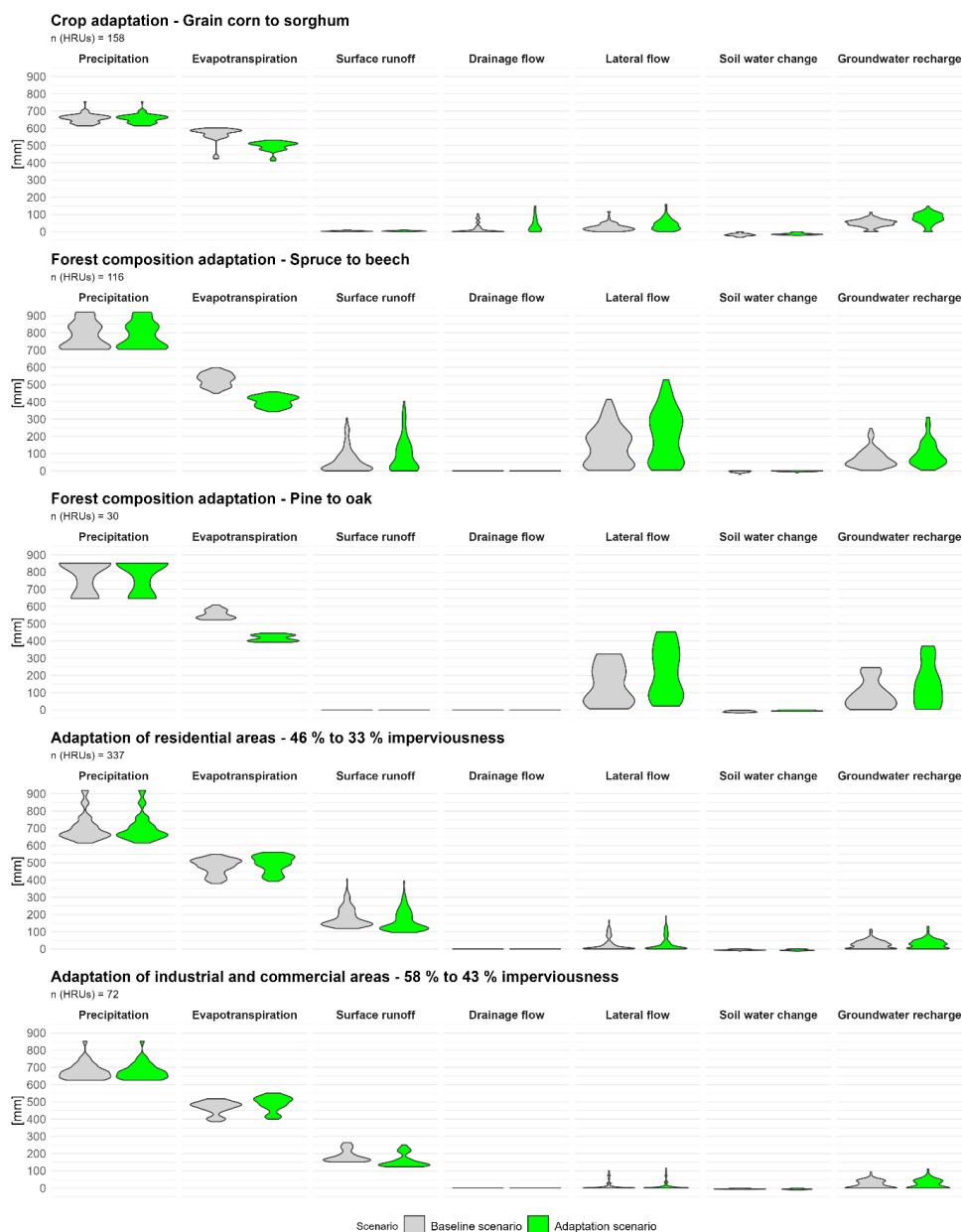
Figure 7: Average annual water balance components from 2011 to 2020 of adapted areas for baseline and adaptation scenarios, area-weighted

475

18

Table 5: Precipitation and water flux coefficients in the base and adaptation scenarios, area-weighted medians

	Scenario	Unit	CORN_SORGHUM	SPRUCE_BEECH	PINE_OAK	URBAN_IMP	INDUSTRY_IMP
Precipitation	all	mm	663	767	851	676	679
Evapotranspiration/ Precipitation	baseline	%	89.0	67.4	68.1	72.1	68.7
	adapted	pp	-11.7	-15.7	-17.2	+1.9	+2.6
Surface runoff/ Precipitation	baseline	%	0.5	2.7	0.0	22.9	26.7
	adapted	pp	0.0	+1.6	0.0	-3.6	-4.1
Drainage flow/ Precipitation	baseline	%	0.0	not drained	not drained	not drained	not drained
	adapted	pp	+3.3				
Lateral flow/ Precipitation	baseline	%	3.6	24.2	9.7	0.4	0.2
	adapted	pp	+2.5	+9.9	+5.2	+0.1	0.0
GW recharge/ Precipitation	baseline	%	8.9	6.5	18.8	3.5	4.4
	adapted	pp	+4.8	+2.4	+10.7	+0.5	+0.2
Soil water change/ Precipitation	baseline	%	-2.9	-0.7	-1.4	-0.9	-0.8
	adapted	pp	+0.6	+0.5	+0.5	-0.1	-0.2

CORN_SORGHUM: Crop adaptation – Grain corn to sorghum
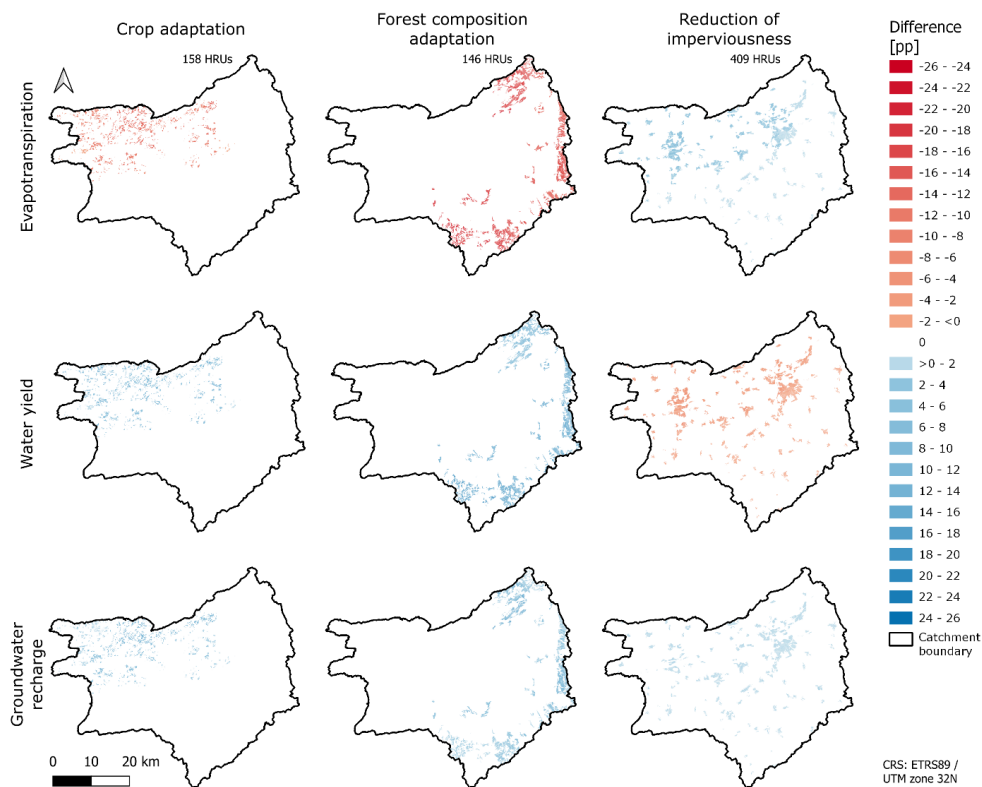SPRUCE_BEECH: Forest composition adaptation – Spruce to beech
PINE_OAK: Forest composition adaptation – Pine to oak
480   URBAN_IMP: Adaptation of residential areas – 46 % to 33 % impervious fraction
INDUSTRY_IMP: Adaptation of industrial and commercial areas – 58 % to 43 % impervious fraction
pp: percentage points

Figure 8: Differences in water flux coefficients between baseline and adaptation scenario by change categories, area-weighted, catchment outline based on GSK3E (LANUV, 2019)

3.2.2 Intra-annual change analysis

The analysis of mean monthly differences over the investigation period in water balance components across the changed land use categories – cropland, forests and built-up areas – reveals distinct hydrologic responses. The area-weighted median temperature and precipitation for each month in the respective areas are shown in Fig. 9a for reference. Monthly temperatures and precipitation follow similar seasonal patterns across the investigated land use categories. However, being mostly concentrated in the catchment's headwaters near the mid-range mountains, the adapted forested areas show higher overall volumes of precipitation and lower temperatures throughout the course of the year.

The replacement of grain corn with sorghum leads to evapotranspiration decreases from May to October, with the largest reductions in August and September (Fig. 9b, left plot). Slight increases in evapotranspiration are simulated for the remainder of the year. Further model outputs (not shown) indicate that the reductions during the growing season are primarily due to decreased plant transpiration, while the increases outside this period are attributed to higher soil evaporation. Groundwater recharge increases consistently throughout the year, showing an inverse relationship with temperature. Drainage flows increase during the winter months (December to March). As Fig. 9c

20

(left plot) illustrates, the relative plant available water content in the topsoil of the investigated agricultural areas reaches nearly 100% during the winter months when temperatures are low. It depletes during the warmer months

505 (April to September), dropping below 50% and even below 30 % in May, July and August indicating water stressed conditions. The substitution of grain corn with grain sorghum leads to higher levels of plant available water during the vegetation period from June to October while no notable differences are modeled from November to April, when the fields remain bare. In April, the modeled plant available water is slightly lower with sorghum than with corn cultivation, reflecting the later planting of sorghum in May and the resulting longer exposure of bare soil.

510 The investigated forest composition adaptations reduce evapotranspiration from September to May, with the most pronounced effects in early autumn (September and October) and spring (March and April) as shown in Fig. 9b (middle plot). From June to August, evapotranspiration increases slightly, reflecting the higher water demand of broad-leaved trees during this period. Lateral flow increases throughout the year, with the largest change values occurring in winter and spring. Groundwater recharge also rises year-round, peaking in spring and late autumn.

515 Surface runoff increases slightly in the period from December to April when the broad-leafed trees are dormant.
In winter, when temperatures are low, the relative plant available water content of the topsoil under coniferous trees reaches 100 % (Fig. 9c, left plot). It follows an annual cycle with critically low levels – below 50 % and even 30 % – occurring during the warmer months (April to September). Through forest composition adaptation towards broad-leafed trees, plant available water increases significantly from April, May and September, reducing the

520 duration of critically low levels by three months. However, the plant-available water still reaches levels indicating water stress from June to August when evapotranspiration is even higher after adaptation.
During the period from October to March only small or no variations in soil moisture content occur.
In built-up areas, changes to water balance components exhibit lower intra-annual variability than in adapted agricultural and forested areas as shown in Fig. 9b (right plot). Reducing impervious surfaces increases

525 evapotranspiration primarily in the warm months from June to October, with the most pronounced increases in July and August. Groundwater recharge remains unchanged from August to November while increases are relatively consistently distributed throughout the rest of the year. Meanwhile, surface runoff decreases year-round, with the greatest reductions occurring in summer. The plant available water in the topsoil follows the seasonal temperature cycle (Fig. 9c, left plot). The reductions of imperviousness lead to slight increases from May to

530 October.
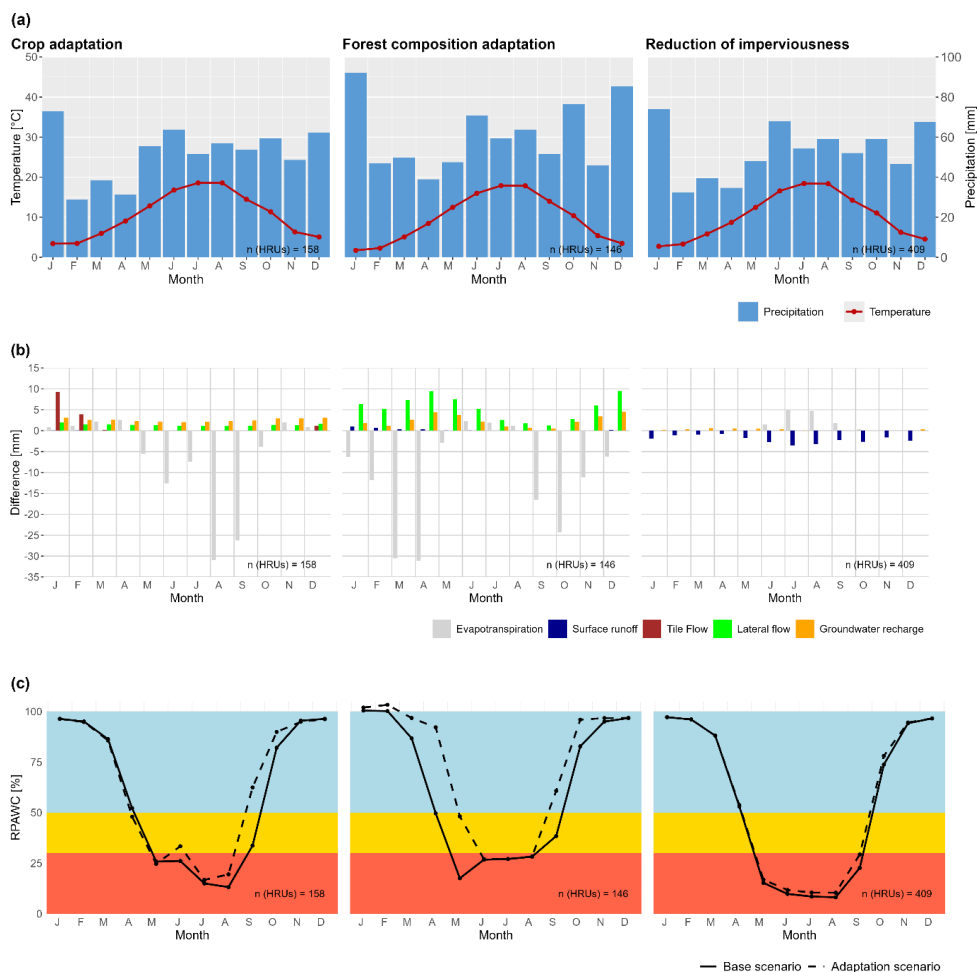
Figure 9: Monthly scenario comparison of mean monthly climate (a), changes of water balance components (b) and relative plant available water content (RPAWC) of the topsoil (300mm) with thresholds of 50% for moderate and 30% for extreme water stress (c) over the investigation period. All data are area-weighted medians of the changed areas.

4 Discussion

4.1 Model performance

The model represents discharge dynamics at the catchment outlet very well in the recession and low flow periods. The model fit of extreme peak flows shows good timing but an overestimation of their magnitude. This is coherent with the applied calibration strategy which was deliberately chosen with a focus on the study of droughts and water retention. It shows that trade-offs occur in the representation of high and low flow by the model. Moreover, the overestimation of discharge peaks by the model can plausibly be related to the flood control reservoirs in the upper catchment. They reduce the highest discharge peaks which would naturally occur with increased magnitude but these anthropogenic streamflow alterations are not considered in the model.

22

The performance metrics at the gauges used for additional spatial validation indicate an overall good representation of streamflow dynamics (Table 4) with PBIAS and NSE values in the range for satisfactory model performance in accordance with the guidelines published by Moriasi et al. (2007). The PBIAS metric also indicates an

550   overestimation of the contribution of the headwaters in mountainous areas (gauge Bentfeld) to the total discharge. These are compensated in the model by underestimated discharges in the lowland catchment when calibrating for the optimal performance for the whole catchment. Therefore, the representation of the water balance of the whole catchment is reasonable while differences in its exact spatial distribution are modeled less accurately, although within reasonable limits.

555   **4.2 Land use adaptation**

The implemented land use adaptations have important hydrologic implications represented by the changes in water fluxes and storage states in the respective areas. The responses are overall consistent with previous studies showing that land management strategies, such as changes in agricultural crops (Placatová et al., 2024; Alves Rodrigues Pinheiro and Nunes, 2023) or forest composition (Bosch and Hewlett, 1982; Cao et al., 2016) have notable impacts

560   on the water balance.

The predicted reduction of evapotranspiration due to crop adaptation (Fig. 7) shows that the reduced water demand of sorghum over corn (Howell et al., 2012) is confirmed by the hydrological model under the study-specific meteorological and site conditions. The underlying difference in model parameters is the reduction in maximum leaf area index (LAI) which is the basis for the calculation of plant transpiration (Neitsch et al., 2011) from 6 for

565   corn to 3 for sorghum (SWAT+ plant database, Bieger et al., 2017). The temporal distribution of the reduction in evapotranspiration, which is concentrated in the warmest months when the climatic water balance is lowest, makes this adaptation measure particularly suitable for stabilizing water fluxes throughout the year. The reduction of evapotranspiration increases water availability for surface runoff and underground water fluxes. Groundwater recharge exhibits the largest increase, followed by lateral flow. Increases of these underground fluxes through

570   storages with relatively long retention times contribute to increased water retention in the landscape. While surface runoff remains unchanged, the highly reactive drainage flow is increased in winter. This is detrimental to increased water retention and it should be further studied whether drainage flow could be reduced by combining the crop adaptations with adaptive drainage management as an additional best management practice. Water storage in the soil profile increases in line with the lower water demand of sorghum compared to corn. The increased soil water

575   also plausibly explains the modeled increases in evaporation from the soil outside of the growing period. The increased plant available water in the topsoil during the vegetation period (Fig. 9c, left plot) underlines the potential of this adaptation measure to reduce water stress in hot and dry summers. While the model results for crop adaptation show that water retention increases, field trials have shown that sorghum cultivation may however not be able to produce comparable amounts of biomass when corn does not experience water stress (Bayerische

580   Landesanstalt für Landwirtschaft, 2024). However, in dry conditions the goals of water management and agricultural productivity are more aligned when drought resilience and thermal requirements of the sorghum coincide (Chadalavada et al., 2021) with their potential for increasing water retention in the catchment. Advances towards adapting sorghum to cooler climates (Schaffasz et al., 2019) can further increase these synergies. Moreover, hydrological considerations and water policies may further incentivize crop adaptation towards

585   increased water efficiency even at the expense of productivity.

To accurately represent forested areas in the model, plant parameters specially adapted to Germany (Müller, 2022) have been applied for the relevant tree species instead of the SWAT+ default database. The replacement of coniferous with broad leafed trees leads to strong reductions of modeled evapotranspiration (Fig. 7) which is consistent with the findings of field experiments with large lysimeters in Germany (Müller, 2005; Landesamt für

590   Natur, Umwelt und Verbraucherschutz, 2018; Harsch et al., 2009; Müller, 2011). The intra-annual distribution (Fig. 9b, middle plot) of the changes is based on the different phenology of the tree species leading to transpiration of broad-leafed trees peaking in summer where changes are minimal and even negative. In the model, this is represented by differences in LAI values, which are higher for broad-leaved trees (beech: 6.7, oak: 5.2) than for coniferous trees (spruce: 6.0, pine: 3.5) outside the dormancy period. During dormancy, LAI values drop

595   significantly for broad-leaved species (oak and beech: 0.01), while coniferous trees retain their foliage (spruce: 5.0, pine: 2.9).

The reduced evapotranspiration allows more water to move vertically in the soil profile as lateral flow or percolate into the groundwater storage. PINE_OAK areas exhibit the largest increase in groundwater recharge, while SPRUCE_BEECH areas show the greatest increase in lateral flow. This contrast is linked to differences in

600   topography, with PINE_OAK areas located in flatter terrain and SPRUCE_BEECH areas in more hilly regions. Similar to the adaptation measures in agricultural areas, these changes in water fluxes increase the retention in the landscape that can contribute to maintaining channel discharge and water levels during dry periods. In SPRUCE_BEECH areas, the surface runoff also increases (Fig. 7) and the intra-annual analysis (Fig. 9b, middle plot) indicates that these changes are concentrated in the leafless months and are therefore plausibly related to the

605   lack of canopy interception in this time period which is also modeled based on LAI (Neitsch et al., 2011). While being surpassed by the increases in lateral flow and groundwater recharge, the increases in surface runoff are detrimental to water retention but could potentially be mitigated by additional water retention measures in the forests (Wilbrand, 2025; Valtera and Schaetzl, 2017; Schüler, 2006). In forested areas, the adaptation measures led to higher soil moisture in the investigation period (Fig. 7). The modelled reduction in soil water content under

610   dry conditions as well as the impacts of the forest composition adaptation are consistent with other studies that use in-situ measurements for validation (Vorobevskii et al., 2024; Boeing et al., 2022).

Driven by the changes in evapotranspiration, the plant available water in the soil is increased in both spring and fall leading to a shortening of the water stressed period (Fig. 9c, middle plot). Spruce trees have been deliberately planted in the *Egge* mountains for economic purposes since 1803 at the cost of the afforestation with native oak

615   and beech trees (Kreis Paderborn, 2024). Especially since 2018, the spruce plantations have been subject to increasing degradation caused by dry periods and bark beetle infestation (Kreis Paderborn, 2024) with damaged areas amounting up to 30 km² in the state-owned forests (Förderverein Nationalpark Senne-Eggegebirge e.V., 2023). Similar trends have been observed in other regions of Germany (Sutmöller and Meesenburg, 2018) with pronounced impacts on hydrology as shown by Wagner et al. (2025). With soil moisture droughts predicted to

620   become more likely in Europe under climate change (Grillakis, 2019; Boeing et al., 2022; Samaniego et al., 2018), this process will be exacerbated. But the subsequent environmental management options cover a wide range from targeted reforestation to rewilding approaches in specially protected areas such as the core zones of the mountainous German national parks *Bayerischer Wald* (Müller, 2022) and *Harz* (Harzer Tourismusverband e.V; Nationalparkverwaltung Harz). This study's results can serve as guidelines for these choices from a hydrologic

625   perspective.

For built-up areas, instead of investigating the widely studied impacts of spatial extent changes, this study focused on the change of impervious fraction of the surfaces which is also known to affect the water balance (Wang et al., 2021). Imperviousness is a SWAT+ model parameter which was adjusted to realistic average values for the study area based on the described remote sensing study of the European Environment Agency (2020b) while the unsealed

630   surface fraction of built-up areas is represented by a plant class for urban green areas with fescue parameters (SWAT+ plant database, Bieger et al., 2017). While not accounting for the small-scale variability of urban spaces, this parameterization allows to model the water balance of built-up areas with similar accuracy than the other investigated land use categories. The periods of modeled soil water scarcity in built-up areas (Fig.9c, right plot) in the summer months should not be interpreted as plants experiencing water stress. In the model, sealed areas and

635   unsealed green areas are lumped together in the same HRUs and therefore no spatial distinction of the soil water that is available to plants is possible.

The modeled decline in surface runoff from built-up areas as well as the increases in groundwater recharge and – to a lesser extent – soil water content under the adaptation scenario confirm the effectiveness of the measures aimed at enhancing infiltration. These results align with previous hydrological studies on the water balance effects

640   of urbanization (Booth and Jackson, 1997). The changes from fast to slow hydrologic fluxes increase the water retention in built-up areas. The modeled increases in evapotranspiration can furthermore provide local cooling effects by promoting latent heat transfers that are important for heat adaptive city planning (Wong et al., 2021).

5 Conclusions

In this study, the eco-hydrological model SWAT+ was applied to investigate the hydrologic impacts of land use-

645   based climate adaptation measures in agricultural, forested and built-up areas during an exceptionally dry period. The ability of the plant model in SWAT+ to accurately represent the impacts of different plant species on the water balance was crucial for conducting this study, which focused on changes within land use classes rather than on their proportional shares in the catchment. A realistic spatial discretization of land use distribution and parameterization was achieved using a combination of external data sources, including agricultural databases,

650   remote sensing products, and prior studies on drainage potential and forest characteristics. This foundation enabled an in-depth assessment of the hydrologic impacts of land use changes under abnormally dry conditions. The calibration strategy which focused on the representation of low-flow periods while maintaining a good overall representation of streamflow dynamics can serve as a blueprint for similar model applications.

Overall, the model results are plausible and consistent with field studies on smaller scales. They indicate that land

655   use strategies promoting infiltration and reducing surface runoff can enhance water retention in the landscape thereby contributing to drought resilience. Furthermore, the modeled land use changes in forested and agricultural areas can contribute to reducing evapotranspiration and strengthening water fluxes through storages with longer retention times. The reduced water demand of the plants in the adapted scenario leads to increases in soil moisture content, thereby decreasing water stress. In built-up areas, the reduction of the impervious fraction increases water

660   retention by strengthening infiltration but also increases evapotranspiration. The latter effect, while not increasing water retention, can improve heat resilience in settlement areas by increasing evapotranspiration as well as water retention by increasing groundwater recharge. These findings emphasize the importance of adaptive land use planning and land management that consider land cover-specific responses to adapt to climatic extremes. Understanding how land use adaptations interact with hydrologic processes can inform sustainable water

665   management strategies, ensuring balanced water distribution in time and space as well as mitigating potential negative impacts of changing climatic conditions. With the current measures being limited at scale by adjusting only the land cover within the same land use class, further investigations should focus additionally on land use transitions and investigate the implications of combined measures on catchment water balance and streamflow dynamics.

670   These results underscore the significant impact of land use adaptations on hydrologic processes, highlighting the potential for management strategies to influence water availability, runoff dynamics, and groundwater recharge across different land cover types. As such they are important nature-based solutions to climate adaptation which need to be recognized by policy makers and administrations alike to establish regulatory and financial frameworks that are conducive to their implementation.

675

Appendices

APPENDIX 1: Land use parameterization with the IACS database

For each agricultural field, the temporally dominant crop was identified by the most frequently planted crop on
680   the field over the seven-year period. If two crops met this condition, the most recent was selected as the dominant
crop. The SWAT+ models' agricultural land use classes from the plant parameter database of SWAT+ were then
assigned based on the IACS data in a stepwise approach shown in Fig. A1. All agricultural areas for which crops
were specified based on the IACS data were superimposed onto agricultural areas in the CORINE 2018 land use
base layer. Remaining agricultural areas in the CORINE 2018 layer that could not be further specified by IACS
685   predominantly contain rural roads and pathways, shrub areas, small forests and other landscape elements (6.96 %
of the catchment area) and were lumped into the range brushland class.
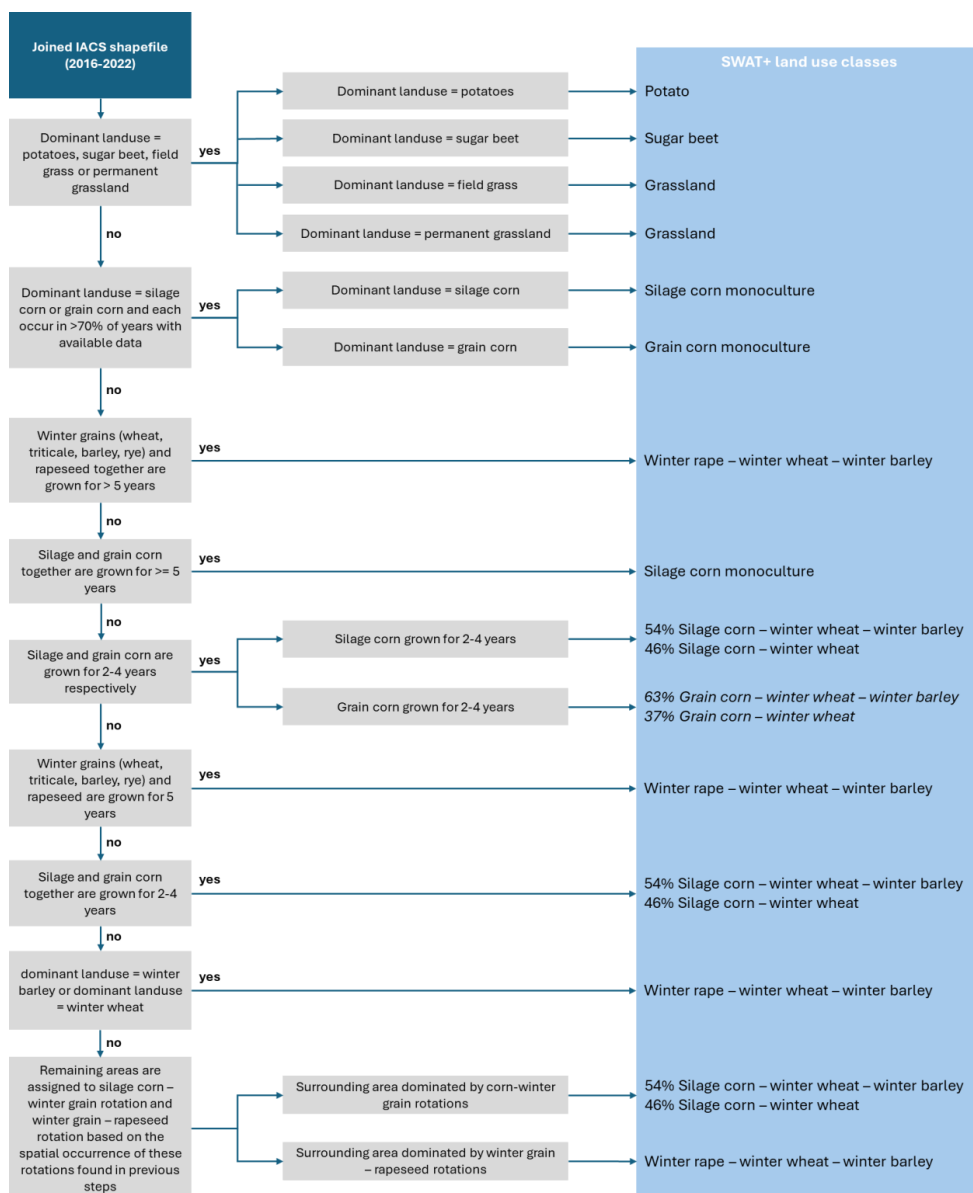
Figure A1: Workflow of the transfer of agricultural land uses derived from the field data of the Integrated Administration and Control System (IACS) data to land use classes for the SWAT+ model

APPENDIX 2: Parameterization of agricultural management operations

695   **Table A1: Tillage operations partially adjusted for the upper Lippe catchment SWAT+ model**

Name	Use	Mixing efficiency [fraction]	Mixing depth [mm]	Roughness [mm]
Plowing	All plowing operations	0.95	270	75
Harrowing	All seedbed preparation operations	0.25	60	20
Cultivating	All deep stubble cultivation operations	0.4	160	20
Roller harrow (default)	Shallow stubble cultivation operations on all crops except corn	0.4	60	5
TripleK (default)	Shallow stubble cultivation operations after corn	0.4	100	25

Table A2: Parameterization of harvest operations adjusted for the upper Lippe catchment SWAT+ model

Operation	Application	Harvest Type	Harvest index [fraction]	Harvest efficiency [fraction]
Grain harvest	Winter wheat, winter barley	grain	0.7	0.95
Rape harvest	Rape	biomass	0.25	0.95
Silage (default)	Silage maize	biomass	0.9	0.95
Hay cut 1	Winter pasture first cut	biomass	0.7	1
Hay cut 2	Winter pasture second cut	biomass	0.65	1
Hay cut 3	Winter pasture third cut	biomass	0.6	1
Hay cut 4	Winter pasture fourth cut	biomass	0.55	1

Note: In SWAT+, the *harvest type* defines whether seed or total above ground biomass are harvested while *harvest*
700   *index* specifies the fraction of the harvested biomass and *harvest efficiency* the fraction of yield biomass removed
by the harvesting equipment, with the remaining yield lost (Neitsch et al., 2011). The *mixing efficiency* specifies
the fraction of materials (residue, nutrients, and pesticides) on the soil surface that are mixed uniformly throughout
the soil depth specified by *mixing depth* and the *roughness* specifies the depth of the surface roughness remaining
after the tillage operation (Neitsch et al., 2011).

705

Table A3a: Agricultural management operations specified for the upper Lippe catchment, multiyear

	Cereals/Oilseed		Grain Corn/Cereals*		Silage Corn/Cereals*		Sorghum/Cereals*	
	Date	Operation	Date	Operation	Date	Operation	Date	Operation
Year 1	Jul. 25	Harvest: **Rape**	Apr. 3	Plow	Apr. 3	Plow	May 10	Plow
	Aug. 9	Rollharrow	Apr. 7	Harrow	Apr. 7	Harrow	May 14	Harrow
	Aug. 23	Cultivate	Apr. 24	Plant: **Corn**	Apr. 24	Plant: **Silage Corn**	May 10	Plant: **Sorghum**
	Oct. 16	Harrow	Oct. 16	Harvest: **Corn**	Sep. 23	Harvest: **Silage Corn**	Oct. 19	Harvest: **Sorghum**
	Oct. 18	Plant: **Wheat**	Oct. 18	TripleK	Oct. 18	TripleK	Oct. 21	TripleK
			Oct. 20	Plow	Oct. 20	Plow	Oct. 22	Plow
			Oct. 22	Rollharrow	Oct. 22	Rollharrow	Oct. 23	Rollharrow
			Oct. 25	Plant: **Wheat**	Oct. 25	Plant: **Wheat**	Oct. 25	Plant: **Wheat**
Year 2	Aug. 9	Harvest **Wheat**	Aug. 9	Harvest: **Wheat**	Aug. 9	Harvest: **Wheat**	Aug. 9	Harvest: **Wheat**
	Aug. 11	Rollharrow	Aug 11	Rollharrow	Aug 11	Rollharrow	Aug. 11	Rollharrow
	Aug. 25	Cultivate	Sep. 5	Cultivate	Sep. 5	Cultivate	Sep. 5	Cultivate
	Sep. 9	Plow	Sep. 9	Plow	Sep. 9	Plow	Sep. 9	Plow
	Sep. 9	Harrow	Sep. 22	Rollharrow	Sep. 22	Rollharrow	Sep. 22	Rollharrow
	Sep. 23	Plant: **Barley**	Sep. 23	Plant: **Barley**	Sep. 23	Plant: **Barley**	Sep. 23	Plant: **Barley**
Year 3	Jul. 14	Harvest: **Barley**	Jul. 14	Harvest: **Barley**	Jul. 14	Harvest: **Barley**	Jul. 14	Harvest: **Barley**
	Jul. 16	Rollharrow	Jul. 16	Rollharrow	Jul. 16	Rollharrow	Jul. 16	Rollharrow
	Aug. 20	Plow	Jul. 23	Plow	Jul. 23	Plow	Jul. 23	Plow
	Aug. 26	Harrow	Jul. 25	Plant: **Clover****	Jul. 25	Plant: **Clover****	Jul. 25	Plant: **Clover****
	Aug. 27	Plant: **Rape**						

* also incorporated as 2-year rotations and single-year monocultures limited to Year 1

** red clover as cover crop, only in multi-year crop rotations

710 **Table A3b: Agricultural management operations specified for the upper Lippe catchment, single year**

	Winter Pasture		Sugar beet	
	Date	Operation	Date	Operation
Year 1	May 5	Harvest: **Hay**	Mar. 9	Harrow
	Jun. 6	Harvest: **Hay**	Apr. 8	Plant: Sugar beet
	Jul. 23	Harvest: **Hay**	Oct. 7	Harvest: Sugar beet
	Sep. 8	Harvest: **Hay**	Oct. 10	Plow

Author contributions

Conceptualization, and Methodology: SG, PW, JK, NF

Funding acquisition: PW, NF

Investigation, Data curation, Formal analysis, and Visualization: SG

715 Supervision, and Validation: PW, JK, NF

Writing (original draft preparation): SG

Writing (review and editing): all authors

Acknowledgements

Competing interests

725 The authors declare that they have no conflict of interest. PW is a member of the editorial board of HESS.

References

Alves Rodrigues Pinheiro, E. and Nunes, M. R.: Long-term agro-hydrological simulations of soil water dynamic
and maize yield in a tillage chronosequence under subtropical climate conditions, Soil and Tillage Research,
229, 105654, doi:10.1016/j.still.2023.105654, 2023.

Arnold, J. G. and Fohrer, N.: SWAT2000: current capabilities and research opportunities in applied watershed
modelling, Hydrological Processes, 19, 563–572, doi:10.1002/hyp.5611, 2005.

Arnold, J. G., Srinivasan, R., Muttiah, R. S., and Williams, J. R.: Large area hydrologic modeling and
assessment part I: model development 1, J American Water Resour Assoc, 34, 73–89, doi:10.1111/j.1752-
1688.1998.tb05961.x, 1998.

Auerswald, K., Geist, J., Quinton, J. N., and Fiener, P.: HESS Opinion: Floods and droughts – Land use, soil
management, and landscape hydrology are more significant drivers than increasing temperatures, 2024.

Ault, T. R.: On the essentials of drought in a changing climate, Science (New York, N.Y.), 368, 256–260,
doi:10.1126/science.aaz5492, 2020.

Bayerische Landesanstalt für Landwirtschaft: Versuchsergebnisse Körnerhirse (Sorghum bicolor),
https://www.lfl.bayern.de/ipz/mais/295682/index.php, 2024.

Beguería, S. and Vicente-Serrano, S. M.: SPEI: Calculation of the Standardized Precipitation-Evapotranspiration
Index, R-Package, 2023.

Berihun, M. L., Tsunekawa, A., Haregeweyn, N., Tsubo, M., Fenta, A. A., Ebabu, K., Bayabil, H. K., and Dile,
Y. T.: Predicting runoff and sediment responses to climate-resilient land use and management scenarios,
Environ Sci Pollut Res, 30, 72262–72283, doi:10.1007/s11356-023-27452-w, 2023.

Bernini, A., Becker, R., Adeniyi, O. D., Pilla, G., Sadeghi, S. H., and Maerker, M.: Hydrological Implications of
Recent Droughts (2004–2022): A SWAT-Based Study in an Ancient Lowland Irrigation Area in Lombardy,
Northern Italy, Sustainability, 15, 16771, doi:10.3390/su152416771, 2023.

Bhattarai, B., Singh, S., West, C. P., Ritchie, G. L., and Trostle, C. L.: Water Depletion Pattern and Water Use
Efficiency of Forage Sorghum, Pearl millet, and Corn Under Water Limiting Condition, Agricultural Water
Management, 238, 106206, doi:10.1016/j.agwat.2020.106206, 2020.

Bieger, K. and Arnold, J. G.: Introduction to SWAT+, A Completely Restructured Version of the Soil and Water
Assessment Tool, Journal of the American Water Resources Association, 53, 115–130, 2017.

Bieger, K., Arnold, J. G., Rathjens, H., White, M. J., Bosch, D. D., Allen, P. M., Volk, M., and Srinivasan, R.:
Introduction to SWAT+, A Completely Restructured Version of the Soil and Water Assessment Tool, J Am
Water Resour Assoc, 53, 115–130, doi:10.1111/1752-1688.12482, 2017.

Blickensdörfer, L., Oehmichen, K., Pflugmacher, D., Kleinschmit, B., and Hostert, P.: Dominant Tree Species
for Germany (2017/2018), Eberswalde, 2022.

Blickensdörfer, L., Oehmichen, K., Pflugmacher, D., Kleinschmit, B., and Hostert, P.: National tree species
mapping using Sentinel-1/2 time series and German National Forest Inventory data, Remote Sensing of
Environment, 304, 114069, doi:10.1016/j.rse.2024.114069, 2024.

Bockholt, K.: Sorghumhirse trotzt Dürre: Anbaufläche in Deutschland steigt langsam, agrarheute.com,
23/12/2020, https://www.agrarheute.com/pflanze/mais/sorghumhirse-trotzt-duerre-anbauflaeche-
deutschland-steigt-langsam-576470#kommentare, last access: 24 April 2025, 2020.

Boeing, F., Rakovec, O., Kumar, R., Samaniego, L., Schrön, M., Hildebrandt, A., Rebmann, C., Thober, S., Müller, S., Zacharias, S., Bogena, H., Schneider, K., Kiese, R., Attinger, S., and Marx, A.: High-resolution drought simulations and comparison to soil moisture observations in Germany, Hydrol. Earth Syst. Sci., 26, 5137–5161, doi:10.5194/hess-26-5137-2022, 2022.

Boergens, E., Güntner, A., Dobslaw, H., and Dahle, C.: Quantifying the Central European Droughts in 2018 and 2019 With GRACE Follow-On, Geophysical Research Letters, 47, doi:10.1029/2020GL087285, 2020.

Booth, D. B. and Jackson, C. R.: URBANIZATION OF AQUATIC SYSTEMS: DEGRADATION THRESHOLDS, STORMWATER DETECTION, AND THE LIMITS OF MITIGATION 1, J American Water Resour Assoc, 33, 1077–1090, doi:10.1111/j.1752-1688.1997.tb04126.x, 1997.

Bosch, J. M. and Hewlett, J. D.: A review of catchment experiments to determine the effect of vegetation changes on water yield and evapotranspiration, Journal of Hydrology, 55, 3–23, doi:10.1016/0022-1694(82)90117-2, 1982.

Bundesanstalt für Geowissenschaften und Rohstoffe: Bodenkundliche Kartieranleitung, 5., verb. und erw. Aufl., Hannover, 438 pp., 2005.

Bundesministerium für Umwelt and Naturschutz, nukleare Sicherheit und Verbraucherschutz: Nationale Wasserstrategie: Kabinettsbeschluss vom 15. März 2023, 120 pp., 2023.

Cao, S., Zhang, J., Chen, L., and Zhao, T.: Ecosystem water imbalances created during ecological restoration by afforestation in China, and lessons for other developing countries, Journal of environmental management, 183, 843–849, doi:10.1016/j.jenvman.2016.07.096, 2016.

Čerkasova, N., White, M., Arnold, J., Bieger, K., Allen, P., Gao, J., Gambone, M., Meki, M., Kiniry, J., and Gassman, P. W.: Field scale SWAT+ modeling of corn and soybean yields for the contiguous United States: National Agroecosystem Model Development, Agricultural Systems, 210, 103695, doi:10.1016/j.agsy.2023.103695, 2023.

Chadalavada, K., Kumari, B. D. R., and Kumar, T. S.: Sorghum mitigates climate variability and change on crop yield and quality, Planta, 253, 113, doi:10.1007/s00425-021-03631-2, 2021.

Deutscher Wetterdienst: Standardized Precipitation Evapotranspiration Index (SPEI): Dokumentation, https://www.dwd.de/DE/fachnutzer/landwirtschaft/dokumentationen/agrowetter/spei.pdf?__blob=publicationFile&v=2, n.d.

Deutscher Wetterdienst: Raster data set of daily maximum and minimum temperatures in °C and sums of precipitation in mm for Germany - HYRAS-DE--TASMAX/-TASMIN/PRE, Version v5.0, https://opendata.dwd.de/climate_environment/CDC/grids_germany/daily/hyras_de/, 2022.

Deutscher Wetterdienst: Phenological observations of crops from sowing to harvest (annual reporters, historical): Version v009, https://opendata.dwd.de/climate_environment/CDC/observations_germany/phenology/annual_reporters/crops/historical/, 2023.

Du, B., Arnold, J. G., Saleh, A., and Jaynes, D. B.: Development and application of SWAT to landscapes with tiles and potholes, Transactions of the ASAE, 48, 1121–1133, doi:10.13031/2013.18522, 2005.

Eini, M. R., Salmani, H., and Piniewski, M.: Comparison of process-based and statistical approaches for simulation and projections of rainfed crop yields, Agricultural Water Management, 277, 108107, doi:10.1016/j.agwat.2022.108107, 2023.

European Environment Agency: Climate change, impacts and vulnerability in Europe 2016: An indicator-based report, European Environment Agency, Luxembourg, EEA report, 1/2017, 2017.

810 European Environment Agency: CORINE Land Cover 2018 (vector), Europe, 6-yearly - version 2020_20u1, May 2020, European Environment Agency, 2020a.

European Environment Agency: Imperviousness Density 2018 (raster 10 m), Europe, 3-yearly, https://land.copernicus.eu/en/products/high-resolution-layer-imperviousness/imperviousness-density-2018, 2020b.

European Environment Agency: European Climate Risk Assessment, 2024.

815 Faustzahlen für die Landwirtschaft, 14. Auflage, Kuratorium für Technik und Bauwesen in der Landwirtschaft e.V. KTBL, Darmstadt, 1180 pp., 2009.

Field, C. B., Barros, V., Stocker, T. F., and Dahe, Q. (Eds.): Managing the Risks of Extreme Events and Disasters to Advance Climate Change Adaptation: Special Report of the Intergovernmental Panel on Climate Change, 1st ed., Cambridge University Press, 2012.

820 Förderverein Nationalpark Senne-Eggegebirge e.V.: Die neuen Wälder der Egge, https://www.egge-nationalpark.de/de/02-Unsere-Region/Die-Egge/lebensraeume/lebensraeume-index.php, 2023.

Gautam, K. and Corzo, G.: Evaluating the impact of ponds on flood and drought mitigation in the Bagmati River Basin, Nepal, Hydrology Research, 54, 1163–1180, doi:10.2166/nh.2023.050, 2023.

Geologischer Dienst NRW: Bodenkarte von Nordrhein-Westfalen 1 50 000 – digital und analog,

825 https://www.gd.nrw.de/pr_kd_bodenkarte-50000.php, 2023.

Grillakis, M. G.: Increase in severe and extreme soil moisture droughts for Europe under climate change, The Science of the Total Environment, 660, 1245–1255, doi:10.1016/j.scitotenv.2019.01.001, 2019.

Haas, H., Reaver, N. G. F., Karki, R., Kalin, L., Srivastava, P., Kaplan, D. A., and Gonzalez-Benecke, C.: Improving the representation of forests in hydrological models, The Science of the Total Environment, 812,

830 151425, doi:10.1016/j.scitotenv.2021.151425, 2022.

Haas, M. B., Guse, B., Pfannerstill, M., and Fohrer, N.: A joined multi-metric calibration of river discharge and nitrate loads with different performance measures, Journal of Hydrology, 536, 534–545, doi:10.1016/j.jhydrol.2016.03.001, 2016.

Hargreaves, G. H. and Samani, Z. A.: Reference Crop Evapotranspiration from Temperature, Applied

835 Engineering in Agriculture, 1, 96–99, doi:10.13031/2013.26773, 1985.

Hari, V., Rakovec, O., Markonis, Y., Hanel, M., and Kumar, R.: Increased future occurrences of the exceptional 2018-2019 Central European drought under global warming, Scientific reports, 10, 12207, doi:10.1038/s41598-020-68872-9, 2020.

Harsch, N., Brandenburg, M., and Klemm, O.: Large-scale lysimeter site St. Arnold, Germany: analysis of 40

840 years of precipitation, leachate and evapotranspiration, Hydrol. Earth Syst. Sci., 13, 305–317, doi:10.5194/hess-13-305-2009, 2009.

Harzer Tourismusverband e.V.: Hintergründe zur Waldsituation, https://www.harzinfo.de/naturlandschaft-harz/initiative-der-wald-ruft/hintergruende.

Herrmann, F. and Wendland, F.: Modellierung des Wasserhaushalts in Nordrhein-Westfalen mit mGROWA:

845 Kooperationsprojekt GROWA+ NRW 2021, LANUV-Fachbericht 110 Teil IIa, Landesamt für Natur, Umwelt und Verbraucherschutz Nordrhein-Westfalen (LANUV), 81 pp., 2021.

Holling, C. S.: Resilience and Stability of Ecological Systems, Annu. Rev. Ecol. Syst., 4, 1–23, doi:10.1146/annurev.es.04.110173.000245, 1973.

850   Hoque, Y. M., Raj, C., Hantush, M. M., Chaubey, I., and Govindaraju, R. S.: How Do Land-Use and Climate Change Affect Watershed Health? A Scenario-Based Analysis, Water Qual Expo Health, 6, 19–33, doi:10.1007/s12403-013-0102-6, 2014.

Howell, T. A., Evett, S. R., Tolk, J. A., Copeland, K. S., Colaizzi, P. D., and Gowda, P. H.: Evapotranspiration of Corn and Forage Sorghum for Silage, American Society of Civil Engineers, 1 pp., 2012.

Jahansouz, M. R., Afshar, R. K., Heidari, H., and Hashemi, M.: Evaluation of Yield and Quality of Sorghum and

855   Millet as Alternative Forage Crops to Corn under Normal and Deficit Irrigation Regimes, Jordan Journal of Agricultural Sciences, 10, 2014.

Jarrett, U., Miller, S., and Mohtadi, H.: Dry spells and global crop production: A multi-stressor and multi-timescale analysis, Ecological Economics, 203, 107627, doi:10.1016/j.ecolecon.2022.107627, 2023.

Kakouei, K., Kiesel, J., Domisch, S., Irving, K. S., Jähnig, S. C., and Kail, J.: Projected effects of Climate-

860   change-induced flow alterations on stream macroinvertebrate abundances, Ecology and evolution, 8, 3393–3409, doi:10.1002/ece3.3907, 2018.

Karki, R., Qi, J., Gonzalez-Benecke, C. A., Zhang, X., Martin, T. A., and Arnold, J. G.: SWAT-3PG: Improving forest growth simulation with a process-based forest model in SWAT, Environmental Modelling & Software, 164, 105705, doi:10.1016/j.envsoft.2023.105705, 2023.

865   Kassaye, S. M., Tadesse, T., Tegegne, G., and Hordofa, A. T.: Quantifying the climate change impacts on the magnitude and timing of hydrological extremes in the Baro River Basin, Ethiopia, Environ Syst Res, 13, doi:10.1186/s40068-023-00328-1, 2024.

Kendall, M. G.: Rank Correlation Methods, Griffin, London, 1955.

Kiniry, J. R., Macdonald, J. D., Kemanian, A. R., Watson, B., Putz, G., and Prepas, E. E.: Plant growth

870   simulation for landscape-scale hydrological modelling, Hydrological Sciences Journal, 53, 1030–1042, doi:10.1623/hysj.53.5.1030, 2008.

Kling, H., Fuchs, M., and Paulin, M.: Runoff conditions in the upper Danube basin under an ensemble of climate change scenarios, Journal of Hydrology, 424-425, 264–277, doi:10.1016/j.jhydrol.2012.01.011, 2012.

Kreis Paderborn: Naturschutzgebiet „Eggekamm": Kulturhistorische Besonderheiten, https://www.kreis-

875   paderborn.de/kreis_paderborn/geoportal/naturschutzgebiete/seiten/eggekamm/kulturhistorische-besonderheiten.php?catID=613171166055, 2024.

Landesamt für Natur, Umwelt und Verbraucherschutz: 50 Jahre Großlysimeteranlage St. Arnold: Entwicklung der Klima- und Wasserhaushaltsgrößen bei unterschiedlicher Vegetation (1965-2014), LANUV-Fachbericht 91, 2018.

880   Landesvermessung NRW: Digitales Geländemodell NW Gitterweite 1m, Geobasis NRW, Bezirksregierung Köln, 2023.

Landwirtschaftskammer Nordrhein-Westfalen: Historische beantragte und als förderfähig festgestellte Teilschläge in NRW, Landwirtschaftskammer Nordrhein-Westfalen, EU-Förderung, 2023.

LANUV: GSK3E Gewässerstationierungskarte des Landes Nordrhein-Westfalen, Landesamt für Natur, Umwelt

885   und Verbraucherschutz, 2019.

Liang, K., Zhang, X., Liang, X.-Z., Jin, V. L., Birru, G., Schmer, M. R., Robertson, G. P., McCarty, G. W., and Moglen, G. E.: Simulating agroecosystem soil inorganic nitrogen dynamics under long-term management

with an improved SWAT-C model, The Science of the Total Environment, 879, 162906, doi:10.1016/j.scitotenv.2023.162906, 2023.

890   Lorenz, R., Stalhandske, Z., and Fischer, E. M.: Detection of a Climate Change Signal in Extreme Heat, Heat Stress, and Cold in Europe From Observations, Geophysical Research Letters, 46, 8363–8374, doi:10.1029/2019GL082062, 2019.

Mann, H. B.: Nonparametric tests against trend, Econometrica, 13, 245–259, 1945.

Marx, A., Kumar, R., Thober, S., Rakovec, O., Wanders, N., Zink, M., Wood, E. F., Pan, M., Sheffield, J., and
895   Samaniego, L.: Climate change alters low flows in Europe under global warming of 1.5, 2, and 3 °C, Hydrol. Earth Syst. Sci., 22, 1017–1032, doi:10.5194/hess-22-1017-2018, 2018.

McKay, M. D.: Sensitivity and uncertainty analysis using a statistical sample of input values, in: Sensitivity and Uncertainty Analysis Using a Statistical Sample of Input Values: Uncertainty Analysis, Ronen, Y. (Ed.), CRC Press, Boca Raton, Florida, 145–186, 1988.

900   McKay, M. D., Beckman, R. J., and Conover, W. J.: A comparison of three methods for selecting values of input variables in the analysis of output from a computer code, Technometrics, 42, 55–61, 2000.

McKee, T. B., Doesken, N. J., and Kleist, J.: The Relationship of Drought Frequency and Duration to Time Scales., 1993.

Menzel, L.: Hydrologische Extreme: Dürren, in: Hydrologie, 1. Auflage, Fohrer, N., Bormann, H., Miegel, K.,
905   Casper, M., Bronstert, A., Schumann, A. H., Weiler, M. (Eds.), UTB basics, 4513, Haupt Verlag, Bern, 223-228, 2016.

Ministerium für Umwelt, Naturschutz und Verkehr NRW: elektronisches wasserwirtschaftliches Verbundsystem für die Wasserwirtschaftsverwaltung in NRW (ELWAS), https://www.elwasweb.nrw.de/elwas-web/data/ow/menge/pegel/pegelDetailsTab.xhtml;jsessionid=6F590982A3F253A68974CFDD9A433015?ci
910   d=1#, 2024.

Mishra, A. K. and Singh, V. P.: A review of drought concepts, Journal of Hydrology, 391, 202–216, doi:10.1016/j.jhydrol.2010.07.012, 2010.

Moriasi, D. N., Arnold, J. G., van Liew, M. W., Bingner, R. L., Harmel, R. D., and Veith, T. L.: Model Evaluation Guidelines for Systematic Quantification of Accuracy in Watershed Simulations, Transactions of
915   the ASABE, 50, 885–900, doi:10.13031/2013.23153, 2007.

Müller, E. V.: Analysis of forest-specific ecosystem services with regard to water balance components: Runoff and groundwater recharge in the forest, Landesforsten Rheinland-Pfalz, Trier, 238 pp., 2022.

Müller, J.: 30 Jahre Großlysimeteranlage in Britz - Zielstellung und Ergebnisse, 11. Gumpensteiner Lysimetertagung, Irdning, 5.-6.04.2005, 29–32, 2005.

920   Müller, J.: The use of lysimeters to determine the water balance in forests in northeastern Germany, Forest Ecology, Landscape Research and Nature Conservation, 37–46, 2011.

Naik, M. and Abiodun, B. J.: Modelling the potential of land use change to mitigate the impacts of climate change on future drought in the Western Cape, South Africa, Theor Appl Climatol, 155, 6371–6392, doi:10.1007/s00704-024-04995-7, 2024.

925   Nash, J. E. and Sutcliffe, J. V.: River flow forecasting through conceptual models part I — A discussion of principles, Journal of Hydrology, 10, 282–290, doi:10.1016/0022-1694(70)90255-6, 1970.

Nationalparkverwaltung Harz: Die Wälder des Nationalparks: Kern einer neuen Wildnis, https://www.nationalpark-harz.de/de/der-nationalpark-harz/lebensraeume/waelder/.

Nauta, S. M., Waterloo, M. J., Gevaert, A. I., Bijl, J. de, and Brotherton, P.: Micro-Catchments, Macro Effects:

930   Natural Water Retention Measures in the Kylldal Catchment, Germany, Water, 16, 733,
       doi:10.3390/w16050733, 2024.

Neitsch, S. L., Arnold, J. G., Kiniry, J. R., and Williams, J. R.: Soil and Water Assessment Tool: Theoretical
       Documentation, Version 2009, 2011.

Northcott, W., Cooke, R. A., Walker, S. E., Mitchell, J. K., and Hirschi, M. C. (Eds.): Modeling Flow on a Tile-

935   Drained Watershed using a GIS integrated DRAINMOD, 2002.

Paez-Trujillo, A., Corzo, G. A., Maskey, S., and Solomatine, D.: Model-Based Assessment of Preventive
       Drought Management Measures' Effect on Droughts Severity, Water, 15, 1442, doi:10.3390/w15081442,
       2023.

Parajuli, P. B., Jayakody, P., Sassenrath, G. F., and Ouyang, Y.: Assessing the impacts of climate change and

940   tillage practices on stream flow, crop and sediment yields from the Mississippi River Basin, Agricultural
       Water Management, 168, 112–124, doi:10.1016/j.agwat.2016.02.005, 2016.

Pfannerstill, M., Guse, B., and Fohrer, N.: Smart low flow signature metrics for an improved overall
       performance evaluation of hydrological models, Journal of Hydrology, 510, 447–458,
       doi:10.1016/j.jhydrol.2013.12.044, 2014.

945   Placatová, R., Papaj, V., Fučík, P., Brázda, J., Pacek, L., and Tlustoš, P.: Evaluation of the Long-Term Water
       Balance in Selected Crop Rotations with Alfalfa in a Soil-Heterogeneous Lowland Region of the Czech
       Republic, Agronomy, 14, 1692, doi:10.3390/agronomy14081692, 2024.

Pohlert, T.: trend: Non-Parametric Trend Tests and Change-Point Detection, R-Package, 2023.

Rakovec, O., Samaniego, L., Hari, V., Markonis, Y., Moravec, V., Thober, S., Hanel, M., and Kumar, R.: The

950   2018–2020 Multi-Year Drought Sets a New Benchmark in Europe, Earth's Future, 10,
       doi:10.1029/2021EF002394, 2022.

Rauthe, M., Steiner, H., Riediger, U., Mazurkiewicz, A., and Gratzki, A.: A Central European precipitation
       climatology. Part I: Generation and validation of a high-resolution gridded daily data set (HYRAS), metz,
       22, 235–256, doi:10.1127/0941-2948/2013/0436, 2013.

955   Razafimaharo, C., Krähenmann, S., Höpp, S., Rauthe, M., and Deutschländer, T.: New high-resolution gridded
       dataset of daily mean, minimum, and maximum temperature and relative humidity for Central Europe
       (HYRAS), Theor Appl Climatol, 142, 1531–1553, doi:10.1007/s00704-020-03388-w, 2020.

Riedel, T., Nolte, C., Beek, T. aus der, Liedtke, J., Sures, B., and Grabner, D.: Niedrigwasser, Dürre und
       Grundwasserneubildung: Bestandsaufnahme zur gegenwärtigen Situation in Deutschland, den

960   Klimaprojektionen und den existierenden Maßnahmen und Strategien, 310 pp., 2021.

Ryan, J. A., Ulrich, J. M., Bennett, R., and Joy, C.: xts: eXtensible Time Series, R package, 2024.

Salomón, R. L., Peters, R. L., Zweifel, R., Sass-Klaassen, U. G. W., Stegehuis, A. I., Smiljanic, M., Poyatos, R.,
       Babst, F., Cienciala, E., Fonti, P., Lerink, B. J. W., Lindner, M., Martinez-Vilalta, J., Mencuccini, M.,
       Nabuurs, G.-J., van der Maaten, E., Arx, G. von, Bär, A., Akhmetzyanov, L., Balanzategui, D., Bellan, M.,

965   Bendix, J., Berveiller, D., Blaženec, M., Čada, V., Carraro, V., Cecchini, S., Chan, T., Conedera, M.,
       Delpierre, N., Delzon, S., Ditmarová, Ľ., Dolezal, J., Dufrêne, E., Edvardsson, J., Ehekircher, S., Forner, A.,
       Frouz, J., Ganthaler, A., Gryc, V., Güney, A., Heinrich, I., Hentschel, R., Janda, P., Ježík, M., Kahle, H.-P.,
       Knüsel, S., Krejza, J., Kuberski, Ł., Kučera, J., Lebourgeois, F., Mikoláš, M., Matula, R., Mayr, S.,
       Oberhuber, W., Obojes, N., Osborne, B., Paljakka, T., Plichta, R., Rabbel, I., Rathgeber, C. B. K., Salmon,

970   Y., Saunders, M., Scharnweber, T., Sitková, Z., Stangler, D. F., Stereńczak, K., Stojanović, M., Střelcová,
       K., Světlík, J., Svoboda, M., Tobin, B., Trotsiuk, V., Urban, J., Valladares, F., Vavrčík, H., Vejpustková, M.,
       Walthert, L., Wilmking, M., Zin, E., Zou, J., and Steppe, K.: The 2018 European heatwave led to stem
       dehydration but not to consistent growth reductions in forests, Nature communications, 13, 28,
       doi:10.1038/s41467-021-27579-9, 2022.

975   Samaniego, L., Thober, S., Kumar, R., Wanders, N., Rakovec, O., Pan, M., Zink, M., Sheffield, J., Wood, E. F.,
       and Marx, A.: Anthropogenic warming exacerbates European soil moisture droughts, Nature Clim Change,
       8, 421–426, doi:10.1038/s41558-018-0138-5, 2018.

       Schaffasz, A., Windpassinger, S., Friedt, W., Snowdon, R., and Wittkop, B.: Sorghum as a Novel Crop for
       Central Europe: Using a Broad Diversity Set to Dissect Temperate-Adaptation, Agronomy, 9, 535,
980   doi:10.3390/agronomy9090535, 2019.

       Schuerz, C.: SWATrunR: Running SWAT2012 and SWAT+ Projects in R, R package, 2024.

       Schüler, G.: Identification of flood-generating forest areas and forestry measures for water retention, Forest
       Snow and Landscape Research, 80, 99–114, 2006.

       Sen, P. K.: Estimates of the Regression Coefficient Based on Kendall's Tau, Journal of the American Statistical
985   Association, 63, 1379, doi:10.2307/2285891, 1968.

       Soetaert, K. and Petzoldt, T.: Inverse Modelling, Sensitivity and Monte Carlo Analysis in R Using Package
       FME, J. Stat. Soft., 33, 1–28, doi:10.18637/jss.v033.i03, 2010.

       Sohn, W., Kim, J.-H., Li, M.-H., Brown, R. D., and Jaber, F. H.: How does increasing impervious surfaces affect
       urban flooding in response to climate variability?, Ecological Indicators, 118, 106774,
990   doi:10.1016/j.ecolind.2020.106774, 2020.

       Sorooshian, S., Duan, Q., and Gupta, V. K.: Calibration of rainfall-runoff models: Application of global
       optimization to the Sacramento Soil Moisture Accounting Model, Water Resources Research, 29, 1185–
       1194, doi:10.1029/92WR02617, 1993.

       Srivastav, A. L., Dhyani, R., Ranjan, M., Madhav, S., and Sillanpää, M.: Climate-resilient strategies for
995   sustainable management of water resources and agriculture, Environmental science and pollution research
       international, 28, 41576–41595, doi:10.1007/s11356-021-14332-4, 2021.

       Statistisches Bundesamt - Destatis: Daten aus dem Gemeindeverzeichnis Kreisfreie Städte und Landkreise nach
       Fläche, Bevölkerung und Bevölkerungsdichte, Gebietsstand: 31.12.2022, 2023.

       Sutmöller, J. and Meesenburg, H.: Einfluss von forstlicher Bestandesentwicklung und Klimawandel auf
1000   Wasserhaushaltskomponenten im Einzugsgebiet der Langen Bramke im Harz, Hydrologie und
       Wasserbewirtschaftung, 62, doi:10.5675/HyWa_2018,3_5, 2018.

       Tetzlaff, B.: Ausweisung potenziell dränierter Flächen unter landwirtschaftlicher Nutzung in Nordrhein-
       Westfalen: LANUV-Fachbericht 110, Kooperationsprojekt GROWA+ NRW 2021, 33 pp., 2021.

       UFZ Helmholtz Zentrum für Umweltforschung: Dürremonitor Deutschland,
1005   https://www.ufz.de/index.php?de=37937, 2024.

       United States Department of Agriculture: Chapter 7 Hydrologic Soil Groups, Part 630 Hydrology, National
       Engineering Handbook., 210-VI-NEH, 2009.

       United States Department of Agriculture: Soil survey manual. USDA Handbook 18. Government Printing
       Office,, Washington, D.C., 2017.

1010 Valtera, M. and Schaetzl, R. J.: Pit-mound microrelief in forest soils: Review of implications for water retention
and hydrologic modelling, Forest Ecology and Management, 393, 40–51, doi:10.1016/j.foreco.2017.02.048,
2017.

van Loon, A. F.: Hydrological drought explained, WIREs Water, 2, 359–392, doi:10.1002/wat2.1085, 2015.

van Vliet, M. T. H., Sheffield, J., Wiberg, D., and Wood, E. F.: Impacts of recent drought and warm years on
1015 water resources and electricity supply worldwide, Environ. Res. Lett., 11, 124021, doi:10.1088/1748-
9326/11/12/124021, 2016.

Vicente-Serrano, S. M., Beguería, S., and López-Moreno, J. I.: A Multiscalar Drought Index Sensitive to Global
Warming: The Standardized Precipitation Evapotranspiration Index, Journal of Climate, 23, 1696–1718,
doi:10.1175/2009JCLI2909.1, 2010.

1020 Vorobevskii, I., Luong, T. T., Kronenberg, R., and Petzold, R.: High-resolution operational soil moisture
monitoring for forests in central Germany, Hydrol. Earth Syst. Sci., 28, 3567–3595, doi:10.5194/hess-28-
3567-2024, 2024.

Wagner, P. D., Kumar, S., and Fohrer, N.: Integrated modeling of global change impacts on land and water
resources, The Science of the Total Environment, 892, 164673, doi:10.1016/j.scitotenv.2023.164673, 2023.

1025 Wagner, P. D., Saba, F., Achanccaray, P., and Fohrer, N.: Drought-induced land use and land cover change
impacts on hydrology: Insights from the Harz mountains, Germany, Hydrol. Earth Syst. Sci., Preprint,
doi:10.5194/egusphere-2025-3091, 2025.

Walker, B., Holling, C. S., Carpenter, S. R., and Kinzig, A. P.: Resilience, Adaptability and Transformability in
Social-ecological Systems, E&S, 9, doi:10.5751/ES-00650-090205, 2004.

1030 Wang, K., Onodera, S., Saito, M., and Shimizu, Y.: Long-term variations in water balance by increase in percent
imperviousness of urban regions, Journal of Hydrology, 602, 126767, doi:10.1016/j.jhydrol.2021.126767,
2021.

Wasserverband Obere Lippe: Hochwasserrückhaltebecken, https://www.wol-
nrw.de/hochwasserschutz/hochwasserrueckhaltebecken/, 2024.

1035 Weiler, M. and Miegel, K.: Globaler und regionaler Wasserkreislauf, in: Hydrologie, 1. Auflage, Fohrer, N.,
Bormann, H., Miegel, K., Casper, M., Bronstert, A., Schumann, A. H., Weiler, M. (Eds.), UTB basics, 4513,
Haupt Verlag, Bern, 2016.

Wilbrand, K.: Identifikation von Potentialen für den dezentralen Wasserrückhalt im Wald, Tag der Hydrologie,
Augsburg, 20/03/2025, 2025.

1040 Wilhite, D. A., Pulwarty, R. S., and Wilhite, D.: Drought and Water Crises, CRC Press, Second edition. | Boca
Raton CRC Press, 2018. | 1st edition published in 2005., 2017.

Wong, N. H., Tan, C. L., Kolokotsa, D. D., and Takebayashi, H.: Greenery as a mitigation and adaptation
strategy to urban heat, Nat Rev Earth Environ, 2, 166–181, doi:10.1038/s43017-020-00129-5, 2021.

Yang, J., Winrich, A., Zhang, T., Qiao, L., Mattingly, C., and Zou, C.: Responses of streamflow to forest
1045 expansion in a typical subhumid watershed under future climate conditions, Journal of environmental
management, 357, 120780, doi:10.1016/j.jenvman.2024.120780, 2024.

Yang, Q. and Zhang, X.: Improving SWAT for simulating water and carbon fluxes of forest ecosystems, The
Science of the Total Environment, 569-570, 1478–1488, doi:10.1016/j.scitotenv.2016.06.238, 2016.

Yapo, P. O., Gupta, H. V., and Sorooshian, S.: Automatic calibration of conceptual rainfall-runoff models:
1050 sensitivity to calibration data, Journal of Hydrology, 181, 23–48, doi:10.1016/0022-1694(95)02918-4, 1996.

Yilmaz, K. K., Gupta, H. V., and Wagener, T.: A process-based diagnostic approach to model evaluation: Application to the NWS distributed hydrologic model, Water Resources Research, 44, doi:10.1029/2007WR006716, 2008.

Zambrano-Bigiarini, M.: hydroGOF: Goodness-of-fit functions for comparison of simulated and observed hydrological time series, Zenodo, 2024.

Zeileis, A. and Grothendieck, G.: zoo: S3 Infrastructure for Regular and Irregular Time Series, J. Stat. Soft., 14, doi:10.18637/jss.v014.i06, 2005.

Zölch, T., Henze, L., Keilholz, P., and Pauleit, S.: Regulating urban surface runoff through nature-based solutions - An assessment at the micro-scale, Environmental research, 157, 135–144, doi:10.1016/j.envres.2017.05.023, 2017.